Myeloid leukemia vulnerabilities embedded in long noncoding RNA locus MYNRL15

Michelle Ng, Lonneke Verboon, Hasan Issa, Raj Bhayadia, Marit Willemijn Vermunt, Robert Winkler, Leah Schüler, Oriol Alejo, Konstantin Schuschel, Eniko Regenyi, Dorit Borchert, Michael Heuser, Dirk Reinhardt, Marie-Laure Yaspo, Dirk Heckl, Jan-Henning Klusmann



PII: S2589-0042(23)01921-1

DOI: https://doi.org/10.1016/j.isci.2023.107844

Reference: ISCI 107844

To appear in: ISCIENCE

Received Date: 19 October 2022

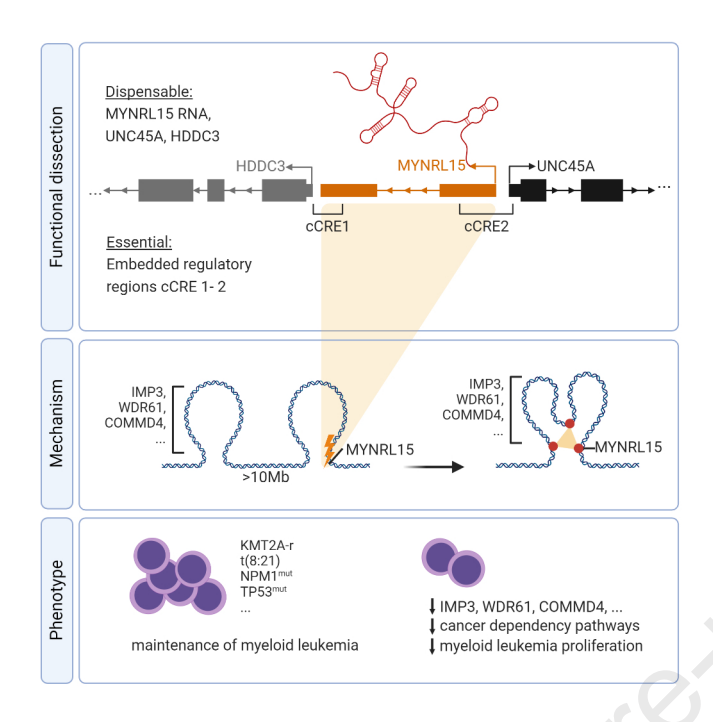
Revised Date: 2 May 2023

Accepted Date: 4 September 2023

Please cite this article as: Ng, M., Verboon, L., Issa, H., Bhayadia, R., Vermunt, M.W., Winkler, R., Schüler, L., Alejo, O., Schuschel, K., Regenyi, E., Borchert, D., Heuser, M., Reinhardt, D., Yaspo, M.-L., Heckl, D., Klusmann, J.-H., Myeloid leukemia vulnerabilities embedded in long noncoding RNA locus *MYNRL15*, *ISCIENCE* (2023), doi: https://doi.org/10.1016/j.isci.2023.107844.

This is a PDF file of an article that has undergone enhancements after acceptance, such as the addition of a cover page and metadata, and formatting for readability, but it is not yet the definitive version of record. This version will undergo additional copyediting, typesetting and review before it is published in its final form, but we are providing this version to give early visibility of the article. Please note that, during the production process, errors may be discovered which could affect the content, and all legal disclaimers that apply to the journal pertain.

© 2023 The Author(s).



Myeloid leukemia vulnerabilities embedded in long noncoding RNA locus MYNRL15

Michelle Ng¹, Lonneke Verboon^{2,3,4}, Hasan Issa^{2,3,4}, Raj Bhayadia^{2,3,4}, Marit Willemijn Vermunt^{2,4}, Robert Winkler^{2,3,4}, Leah Schüler^{2,3,4}, Oriol Alejo¹, Konstantin Schuschel^{2,3,4}, Eniko Regenyi^{1,5}, Dorit Borchert⁶, Michael Heuser⁷, Dirk Reinhardt⁸, Marie-Laure Yaspo⁵, Dirk Heckl^{9*}, Jan-Henning Klusmann^{2,3,4,10*}

- ¹ Department of Pediatric Hematology and Oncology, Martin Luther University Halle-Wittenberg, 06120 Halle (Saale), Germany
- ² Department of Pediatrics, Goethe University Frankfurt, 60323 Frankfurt (Main), Germany
- ³ Frankfurt Cancer Institute, Goethe University Frankfurt, 60323 Frankfurt (Main), Germany
- ⁴ German Cancer Consortium (DKTK), Partner Site Frankfurt/Mainz and German Cancer Research Center (DKFZ), Heidelberg, Germany
- ⁵ Department of Vertebrate Genomics, Max Planck Institute for Molecular Genetics, 14195 Berlin, Germany
- ⁶ Department of Pediatric Hematology and Oncology, Hannover Medical School, 30625 Hannover, Germany
- Department of Hematology, Hemostasis, Oncology and Stem Cell Transplantation, Hannover Medical School, 30625 Hannover, Germany
- ⁸ Clinic for Pediatrics III, University Hospital Essen, 45147 Essen, Germany
- ⁹ Institute for Experimental Pediatric Hematology and Oncology, Goethe University Frankfurt, 60323 Frankfurt (Main), Germany
- ¹⁰ Lead contact
- * These authors contributed equally

Running title:

MYNRL15 in myeloid leukemia

Keywords:

Long noncoding RNA, myeloid leukemia, CRISPR, chromatin architecture

Correspondence:

Prof. Dr. Jan-Henning Klusmann (jan-henning.klusmann@kgu.de; +49 69 6301 5094) or Prof. Dirk Heckl (d.heckl@kinderkrebsstiftung-frankfurt.de; +49 69 6786 6558).

Abstract word count	150
Main text word count	3543
# Figures	5
# Supplementary figures	7
# Supplementary tables	6
# References	76

Summary

The noncoding genome presents a largely untapped source of new biological insights, including thousands of long noncoding RNA (IncRNA) loci. While IncRNA dysregulation has been reported in myeloid malignancies, their functional relevance remains to be systematically interrogated. We performed CRISPRi screens of IncRNA signatures from normal and malignant hematopoietic cells and identified *MYNRL15* as a myeloid leukemia dependency. Functional dissection suggests an RNA-independent mechanism mediated by two regulatory elements embedded in the locus. Genetic perturbation of these elements triggered a long-range chromatin interaction and downregulation of leukemia dependency genes near the gained interaction sites, as well as overall suppression of cancer dependency pathways. Thus, this study describes a new noncoding myeloid leukemia vulnerability and mechanistic concept for myeloid leukemia. Importantly, *MYNRL15* perturbation caused strong and selective impairment of leukemia cells of various genetic backgrounds over normal hematopoietic stem and progenitor cells *in vitro*, and depletion of patient-derived xenografts *in vivo*.

Introduction

15

16

17

18

19

20

21

22

23

24

25

26

27

28

29

30

31

32

33

34

35

36

37

38

39

40

41

Noncoding sequences comprise 98% of the human genome and harbor a multitude of functional units, including regulatory elements and diverse species of small and long noncoding RNA (IncRNA) loci¹. Emerging evidence has implicated growing numbers of these noncoding units as players in a variety of physiological and disease processes, including in cancer^{2,3}. This represents a major opportunity for biologic and therapeutic discovery, especially for malignancies like acute myeloid leukemia (AML), whose treatment has only recently begun to evolve beyond the cytostatic regimen developed in the 1970s4. Studies in AML patient cohorts have uncovered IncRNA expression signatures specific to genetic subgroups of AML⁵⁻⁷ as well as unifying stem cell signatures^{6,8}. However, due to their extensive mechanistic diversity⁹, the study of IncRNAs can be more complicated than of other noncoding RNA species, and only a handful of IncRNA loci have undergone extensive functional characterization in AML¹⁰⁻¹³. Thus, despite rapid growth in the field, our knowledge of lncRNA loci and their roles in this disease remains severely limited. Loosely defined as noncoding transcripts longer than 200 nucleotides, a significant barrier in the characterization of IncRNAs has been the difficulty of unraveling their mechanisms of action. LncRNA loci can occur sense- or antisense-overlapping, head-to-head, or intergenic in relation to protein-coding genes, and besides RNA-mediated cis and trans action, they can exert cis-regulatory effects independent of the transcript itself, through the act of transcription at the locus or through DNA regulatory elements embedded in the locus9. In addition, transcriptional regulatory units such as enhancers and promoters can initiate bidirectional transcription, and considerable overlap exists between IncRNA loci and regulatory regions¹⁴. These mechanisms are also not mutually exclusive, and some lncRNA loci may act through multiple routes. One prominent example is PVT1, a lncRNA in the MYC locus, which acts as a bona fide oncogenic RNA while its promoter functions as a tumour suppressor boundary element¹⁵. Thus, in-depth functional dissection is required to fully understand the functions of uncharacterized IncRNAs.

In this study, we set out to identify IncRNAs involved in myeloid leukemia pathogenesis via a CRISPR interference (CRISPRi) screen of expression signatures derived from normal hematopoietic cells and pediatric AML patient samples. Detailed characterization of the top candidate from the screen, *MYNRL15*, suggested an RNA-independent mechanism via two candidate regulatory regions embedded in the locus. Genetic perturbation of these elements was associated with long-range chromatin conformation changes and downregulation of cancer dependency pathways. Importantly, *MYNRL15* perturbation selectively impaired AML cells of multiple genetic backgrounds compared to normal hematopoietic stem and progenitor cells (HSPCs) *in vitro*, and depleted AML xenografts *in vivo*. Thus, we report a new noncoding vulnerability and mechanistic concept for myeloid leukemia.

Results

Systematic interrogation of HSPC/AML IncRNAs via CRISPRi screens

We previously developed a noncoding RNA expression atlas of the human blood system encompassing hematopoietic stem cells (HSCs) and their differentiated progeny, as well as pediatric AML samples⁶. In addition to stem cell signatures reminiscent of those previously established for protein-coding genes^{16,17}, we discovered progenitor- and AML subtype-associated lncRNA profiles that could potentially serve as leukemia-specific targets, given their absence in HSCs (Figure 1a). To probe this resource for functionality and identify myeloid leukemia vulnerabilities, we conducted a CRISPRi-based dropout screen of 463 lncRNA genes from 8 distinct signatures in 6 human leukemia cell lines (Figure 1b). Five cell lines were selected to represent prominent cytogenetic subgroups of AML – ML-2, NOMO-1 (*KMT2A*-rearreanged), SKNO-1, KASUMI-1 (standard risk with t[8:21]), M-07E (high risk with inv[16]) – and we also included the well-studied erythroleukemia line K562. Stable dCas9-KRAB expressing cell lines were transduced with a sgRNA library targeted to lncRNA transcription start sites (Table S1; see Methods for design principles), and sgRNA abundances were quantified via next generation sequencing before and after 18 population doublings.

69

70

71

72

73

74

75

76

77

78

79

80

81

82

83

84

85

86

87

88

89

90

91

92

93

94

Model-based analysis of genome-wide CRISPR-Cas9 knockout (MAGeCK)¹⁸ was used to call essential lncRNAs required for leukemia cell proliferation. While most lncRNA dependencies were identified in only one cell line, consistent with previously reported lncRNA screens^{19,20}, several were called in two or more cell lines, including *SNAI3-AS1*, *NIPBL-AS1*, *VENTXP7*, *AC079779.5*, and *AC068831.3* (Figure 1c, Figure S1a, Table S1).

Identification of MYNRL15 as a myeloid leukemia dependency locus

Because it emerged as the top candidate overall from our screen, we subsequently focused on AC068831.3 (ID: ENSG00000224441 in Ensembl v85 [release 07/2016]) (Figure 1c, Figure S1a-b) - hereafter referred to as MYNRL15 (myeloid leukemia noncoding regulatory locus on chromosome 15). We validated the anti-leukemic effect of MYNRL15 knockdown in individual proliferation assays, using three effective sgRNAs in all 6 cell lines (Figure S1c-d; note, one library sgRNA did not achieve efficient knockdown and was replaced). MYNRL15 is a low-abundance, nuclear-enriched transcript (Figure 1d-e) from the GMP/AML signature (Figure 1a, Figures S2a-c). It is transcribed from chromosome 15, where it is flanked by two protein-coding genes: UNC45A and HDDC3 (Figure 2a). Given the effect of the CRISPRi system on the expression of these neighbouring genes (Figure 2b, Figure S1c right), a range of gain- and loss-of-function approaches were necessary to delineate the source of the MYNRL15 knockdown phenotype (Figure 2, Figure S2). Whereas CRISPR mediated excision of MYNRL15 using dual sgRNA vectors recapitulated the effect produced by CRISPRi, targeting the transcript via shRNAs and LNA-gapmeRs had little impact on proliferation (Figure 2c, Figure S2a-b), as did CRISPR mediated promoter excision and splice site disruption (Figure 2c, Figure S2c and S2e). Both protein-coding neighbours also appeared to be dispensable, as determined by individual and combined CRISPR-Cas9 mediated knockout of UNC45A and HDDC3, as well as CRISPRi mediated knockdown of HDDC3 (Figure 2c, Figure S2b-c, Figure S2e). Overexpression of MYNRL15 cDNAs additionally failed to rescue the CRISPRi knockdown phenotype (Figure 2d). Taken together, these data indicate that neither of the flanking protein-coding genes, nor the MYNRL15 transcript itself, is responsi-

96

97

98

99

100

101

102

103

104

105

106

107

108

109

110

111

112

113

114

115

116

117

118

119

120

121

ble for the function of the locus in myeloid leukemia cells. Rather, they suggest that *MYNRL15* acts as an expressed noncoding regulatory locus with RNA-independent function.

Functional dissection of the MYNRL15 locus reveals crucial regulatory regions

Given the apparent dispensability of UNC45A, HDDC3, and the MYNRL15 transcript itself in leukemia cells, we hypothesized that MYNRL15 may harbor DNA regulatory elements which drive its leukemia dependency phenotype. To test this hypothesis, we functionally dissected the MYNRL15 locus via complementary CRISPRi and CRISPR-Cas9 screens tiling a 15 kb area centered on MYNRL15. Cell lines (K562, ML-2, M-07E, KASUMI-1) stably expressing either dCas9-KRAB or Cas9 were transduced with a sgRNA library covering the region at a mean density of 0.11 sgRNAs per bp (Table S2), with the expectation that key areas would be demarcated by hubs of depleting sgRNAs. Notably, the MYNRL15 locus contains several regions that exhibit features characteristic of cis-regulatory elements, such as H3K4Me1 and H3K27Ac histone marks, DNase hypersensitivity, and transcription factor occupancy including multiple CTCF and cohesin binding sites (Figure 3a). The tiling screens uncovered two regions where accessibility and integrity were required by the leukemia cells, both of which overlapped CpG islands and divergent H3K27Ac/H3K4me1 signals (Figure 3b, Figure S3a). Both regions enhanced reporter gene expression, singly and in combination, when cloned upstream of a minimal promoter in dual luciferase assays (Figure S3b). Together, these data nominate the crucial regions as functional sequences and candidate *cis*-regulatory elements (cCREs C1 and C2). The Cas9 based mutagenesis strategy also reiterated that leukemia cells do not seem particularly dependent on the UNC45A and HDDC3 coding sequences, indicating that local enhancer functions on these genes are unlikely to explain the antileukemic effect of *MYNRL15* perturbation.

RNA profiling suggests regulation of cancer dependency pathways by MYNRL15

Aiming to identify the target genes and pathways controlled by the *MYNRL15* locus, we next performed RNA sequencing following the disruption of cCREs C1 and C2 via CRISPR-Cas9 mediated induction of DNA double-strand breaks (hereafter referred to simply as *MYNRL15*

123

124

125

126

127

128

129

130

131

132

133

134

135

136

137

138

139

140

141

142

143

144

145

146

147

148

perturbation). We opted for the CRISPR-Cas9 system in an effort to achieve a narrower perturbation of MYNRL15 and mitigate the longer-range suppression caused by CRISPRi; however, expression of the neighboring genes UNC45A and HDDC3 were still affected (Figure S4c). We selected two guides from each cCRE, all of which robustly depleted K562 and ML-2 leukemia cells (Figure 3c). This phenotype was underpinned by global changes in gene expression (Figure 3d-f, Figure S4a-c), including the dramatic suppression of cancer dependency signatures related to proliferation and metabolism across both cell lines and two time points (Figure 3e-f, Figure S4c). 531 genes were commonly deregulated across both K562 and ML-2 cells (167 up, 364 down), including 20 downregulated genes from chromosome 15 (Figure 3d). The downregulated genes were enriched for ontology terms related to the ribosome and RNA splicing (Figure 3e) - an observation that was confirmed by GSEA (Figure 3f), implicating MYNRL15 in the maintenance of these processes. GSEA further revealed suppression of other cancer-essential pathways such as oxidative phosphorylation and DNA replication, as well as of well-known oncogenic programs such as MYC target genes, upon MYNRL15 perturbation (Figure 3f). However, while these data support MYNRL15's leukemia dependency phenotype, they represent general pathways and no obvious candidate targets stood out (e.g. outstanding fold change and significance, known cancer genes, near the locus), leading us to consider the possibility that the locus may regulate multiple genes in a genomic neighborhood²¹ in a subtler manner. To explore this alternative, we applied a sliding window approach to GSEA by using custom gene sets comprised of 1 Mb, 2 Mb, 5 Mb, and 10 Mb sections of chromosome 15 (see Methods for details). This revealed positional gene sets that were deregulated following MYNRL15 perturbation, including the area around MYNRL15 and a distal region in both K562 and ML-2 (Figure 3g, Figure S4d), and others that were unique to one of the cell lines (Figure S4e).

Altered chromosome 15 architecture underlies the MYNRL15 perturbation phenotype
Given the deregulation of chromosome 15 neighborhoods upon MYNRL15 perturbation, we
explored whether this may be associated with changes in chromatin conformation using next

150

151

152

153

154

155

156

157

158

159

160

161

162

163

164

165

166

167

168

169

170

171

172

173

174

175

generation Capture-C (NG Capture-C)²². **Because** of the strong divergent H3K27Ac/H3K4me1 signal, the CTCF binding site overlapping the element, and the potent perturbation phenotype (Figure 3b-c), we focused on MYNRL15 cCRE C1 and used enrichment probes complementary to this region. In unedited K562 and ML-2 cells, Capture-C revealed extensive local interactions between the MYNRL15 locus and sequences within a 500 kb radius, with almost no interactions occurring outside of a 2 Mb radius (Figure 4a-c). Interestingly, MYNRL15 perturbation had little impact on this local interaction profile, and instead caused the gain two long-range interactions 12 Mb and 15 Mb away from the locus (Figure 4b-d), indicating larger-scale reorganization of chromosome 15 upon MYNRL15 perturbation that brings the locus into contact with distal sites. Notably, both the local and gained long-range interactions overlap with contact domain boundaries (Figure 4b-c, Figure S5a-b). Interestingly, in K562 ChIP-seq data from ENCODE, 24 transcription factors show occupancy in both C1 and C2 (Figure 4e, Table S3). Of these, 9 also bind both gained interaction sites, of which 8 have been described to function in hematopoiesis or leukemia (see Table S3 for PMIDs). We think these would be the most likely candidates for the mediator of the long-range interaction, and this list may serve as a starting point for future studies. Given the gained long-range chromatin interactions following MYNRL15 perturbation, we hypothesized that this distal region may be the source of its anti-leukemic phenotype. To probe the region for candidate effectors of the phenotype, we conducted a CRISPR-Cas9 knockout screen of its 29 protein-coding genes (Table S4) and cross-referenced the results with differentially expressed genes identified by RNA sequencing (Figure 3f). Thus, by integrating chromatin conformation, transcriptome, and leukemia dependency information, we found several candidate downstream effector genes of MYNRL15 perturbation: IMP3, WDR61, COMMD4, and SNUPN (Figure 4f, Figure S6c). These genes belong to the gained chromatin interaction region, are downregulated following MYNRL15 perturbation, and score as leukemia dependencies in the CRISPR-Cas9 knockout screen, suggesting that they contribute to the anti-leukemic phenotype triggered by MYNRL15 perturbation. In contrast, in the

177

178

179

180

181

182

183

184

185

186

187

188

189

190

191

192

193

194

195

196

197

198

199

local region around MYNRL15 (Figure 3g; this gene set is downregulated in GSEA), downregulated and dependency genes are mutually exclusive and are thus unlikely to underlie the anti-leukemic phenotype (Figure S6d; gene essentiality data from DepMap²³). We note that, genome-wide, over 200 dependency genes belonging to crucial cellular pathways are downregulated after MYNRL15 perturbation (Figure 4g). The gained chromatin interaction and suppression of *IMP3*, *WDR61*, *COMMD4*, etc. may only be a part of this broad deregulation. To validate the results of the gained interaction region screen, we performed CRISPR-Cas9 knockout of the top candidates, IMP3 and WDR61, and confirmed that guides targeting these genes depleted K562 and ML-2 cells at a level comparable to MYNRL15 perturbation (Figure S6e). IMP3 encodes a component of the 60-80S U3 small nucleolar ribonucleoprotein that is required for early cleavages in pre-18S ribosomal RNA processing²⁴. WDR61 encodes a subunit of the PAF1 complex (PAF1c), which has been reported to stimulate the transcriptional activity of KMT2A and KMT2A-rearranged fusion oncoproteins at HOX loci^{25,26}. Of note, among the expression changes associated with MYNRL15 perturbation, signatures related to ribosome biogenesis and function were strongly suppressed (Figure 3e-f), and signatures induced by Paf1c inactivation²⁷ – including the downregulation of Hoxa9 and Meis1 target genes – were also detected (Figure S6f). In summary, genetic perturbation of MYNRL15 C1 triggered the formation of a long-range chromatin interaction and the downregulation of several leukemia dependency genes in the distal region. This was associated with the suppression of pro-leukemic PAF1C targets ribosome-related signatures, among other crucial pathways. These results implicate MYNRL15 in the maintenance of a permissive chromatin conformation in leukemic cells that assures expression of cancer dependency genes (Figure 4f), although the mediating factor remains unknown.

201

202

203

204

205

206

207

208

209

210

211

212

213

214

215

216

217

218

219

220

221

222

223

224

225

Anti-leukemic effect of MYNRL15 perturbation in primary cells

MYNRL15 perturbation had anti-leukemic effects across cell lines representative of the wide spectrum of genetic alterations found in AMLs (Figures 1a and 3b, Figure S1, Table S5), including those important to adult AMLs such as NB-4 (PML:RARA), OCI-AML3 (normal karyotype with NPM1 and DNMT3A mutations), and TF-1 (normal karyotype with TP53) (Figure S7a). To evaluate whether MYNRL15 dependency is specific to leukemic cells, we leveraged all-in-one lentiviral CRISPR-Cas9 constructs in primary human CD34⁺ hematopoietic stem and progenitor cells (HSPCs) from healthy donors and in blasts derived from two different AML patients (see Table S5 for patient characteristics). The cells were transduced with vectors containing MYNRL15-targeting or control sgRNAs, sorted, and seeded in methylcellulose-based media colony-forming assays. Whereas MYNRL15 perturbation moderately impaired colony formation in CD34+ HSPCs, it had little effect on their replating capacity or differentiation (Figure 5a). In contrast, AML colony-forming units were virtually eradicated across three subgroups of pediatric AML and normal karyotype adult AML samples (8 samples total; Figure 5b-d), implying that MYNRL15 perturbation selectively impacts AML cells, and outlining a possible therapeutic window (Figure 5e). Interestingly, we note the presence of interactions between the MYNRL15 locus and distal upstream regions in CD34+ HSPCs (Figure S7b), suggesting that pre-existing long-range connectivity may contribute to the attenuated effect of MYNRL15 perturbation in these cells. Altogether, our data suggest that the MYNRL15 locus is broadly required by myeloid leukemia cells of different subgroups and genetic backgrounds. To assess the anti-leukemic effect of MYNRL15 perturbation in vivo, we applied CRISPRibased two-color competitive xenotransplantation assays using AML cell lines and patientderived xenografts (PDXs) (Figure 5f, see Table S5 for patient characteristics). Importantly, MYNRL15 perturbation impaired the propagation of two AML cell lines and two PDXs in recipient mice (Figure 5f, Figure S7c-d), confirming its capacity to deplete leukemic cells in *vivo*. Combined with its selective impairment of AML cells, these results provide a proof-of-principle of how *MYNRL15* perturbation may be leveraged as a therapeutic concept.

Discussion

226

227

228

229

230

231

232

233

234

235

236

237

238

239

240

241

242

243

244

245

246

247

248

249

250

251

The discovery of functional noncoding loci and subsequent efforts to uncover their functions have led to new insights in a range of pathophysiological contexts. Here, we present a systematic exploration of IncRNA loci in myeloid leukemia, starting from HSPC / AML signatures from a patient cohort, proceeding through screens and extensive functional studies, and concluding with experiments in primary cells. We describe a previously uncharacterized IncRNA locus that is required by myeloid leukemia cells from various cytogenetic and mutational backgrounds: MYNRL15 (myeloid leukemia noncoding regulatory locus on chromosome 15). By integrating several lines of evidence, we implicate elements embedded in the MYNRL15 locus in the RNA-independent regulation of cancer dependency pathways and long-range chromatin architecture. To our knowledge, this is the first functionally relevant RNA-independent IncRNA locus reported in myeloid leukemia. Notably, MYNRL15 perturbation showed strong anti-leukemic effects in primary AML cells of different genetic backgrounds, implying therapeutic interest, which we validated with proof-of-principle in vivo experiments using AML PDXs. In our study, MYNRL15 perturbation resulted in the formation of a long-range chromatin interaction and downregulation of cancer dependency genes, including several in the gained interaction region. The range of the gained interaction (12-15 Mb away from the MYNRL15 locus) is far greater than what is described in the literature for topologically associating domain (TAD) fusion²⁸⁻³⁰ or enhancer-promoter loops³¹. It is unclear what large-scale chromatin re-organization mechanism could be responsible for bringing the MYNRL15 locus into contact with this distal site. However, we identified 9 potential transcription factors that may mediate the interaction, based on their occupancy of MYNRL15's C1/C2 regions and the distal interaction sites.

253

254

255

256

257

258

259

260

261

262

263

264

265

266

267

268

269

270

271

272

273

274

275

276

277

278

We note that, while there is considerable overlap between enhancer RNA (eRNA) and IncRNA annotations¹⁴, and while some of our data support a local enhancer-like function for MYNRL15, we did not find evidence for locally-driven phenotypes or RNA function. We cannot completely exclude the possibility that MYNRL15 may act as an enhancer on nearby genes, but based on integrative differential expression and leukemia dependency analyses, it seems unlikely that these local transcriptional effects are responsible for the strong antileukemic phenotype triggered by MYNRL15 perturbation. The long-range architectural changes and associated downregulation of leukemia dependency genes at the distal interaction sites represent our most compelling lead on candidate targets of the MYNRL15 locus. Given the attenuated impact of MYNRL15 perturbation on normal HSPCs compared to AML cells, we speculate that distal connectivity may be the native conformation of the locus that is lost during leukemic transformation; thus, re-introducing it would selectively impair leukemic cells. The oncogenic rewiring of 3D chromatin architecture through mutations and structural variants has been reported in cancer^{30,32-35}. However, it is unlikely that genetic alteration underlies MYNRL15's role in leukemia, since the locus is required by cells from varied cytogenetic and mutational backgrounds. We speculate instead that MYNRL15 may be involved in unifying leukemic genome organization signatures similar to the phenomenon of stemnessrelated expression and epigenetic signatures 16,36,37. Recent studies have begun to implicate aspects of chromatin architecture in cell state transitions during hematopoiesis³⁸⁻⁴² and in the maintenance of leukemic transcription programs⁴³⁻⁴⁶. Future studies may further reveal leukemic 3D genome organization signatures that underpin general oncogenic behaviors, irrespective of mutational drivers. Such signatures may be ideal targets for the development of

Limitations of the study

In this study, we implicate *MYNRL15* in the RNA-independent regulation of chromatin architecture and cancer dependency pathways in myeloid leukemia. Although we observed gained long-range interactions following *MYNRL15* perturbation, and downregulation of key

cancer-specific therapies, especially if they are common across different genetic subtypes.

280

281

282

283

284

285

286

287

288

301

genes near the gained interaction sites, the exact mechanism remains elusive. As discussed above, while we cannot completely exclude a local enhancer-like role for *MYNRL15*, we suspect that the long-range chromatin interaction involving *IMP3*, *WDR61*, *COMMD4*, etc. is the most relevant part of its leukemia dependency. Further investigation into genome-wide chromatin conformation (e.g. using Hi-C) or co-localization assays (e.g. FISH) may shed light on what large-scale reorganization occurs upon *MYNRL15* perturbation to bring the locus into contact with the distal interaction sites. In addition, pulldown, immunoprecipitation and/or proteomic studies may help identify the transcription factor(s) that mediate this interaction.

Acknowledgements

- We thank D. Downes and J. R. Hughes (MRC Weatherall Institute, Oxford) for providing the
- NG Capture-C protocol and consulting on experimental design. We also thank A. Schwarzer,
- 291 F. F. Adams (Hannover Medical School), V. Amstislavskiy (Max Planck Institute for Molecu-
- 292 Iar Genetics), and J. L. Mateo (University of Oviedo) for bioinformatics guidance, and A. Ko-
- vacsovics (Max Planck Institute for Molecular Genetics), A. Navarrete Santos, L. Gack, K.
- 294 Huke, K. Menge, C. Beyer (Martin Luther University Halle-Wittenberg), and F. Kalensee
- 295 (Goethe University Frankfurt) for technical assistance.
- 296 This work was supported by the following funding: J.H.K. European Research Council
- 297 Horizon 2020 program (#714226), Hilfe für krebskranke Kinder Frankfurt e.V., St. Baldrick's
- 298 Robert Arceci Innovations Award; D.H. German Cancer Aid (#111743); M.N. Hannover
- 299 Biomedical Research School stipend.
- 300 Illustrations and the graphical abstract were created with BioRender.com.

Author contributions

- M.N., L.V., H.I., R.B., R.W., L.S. O.A., and D.B. performed experiments and analyzed the
- results. M.N., K.S., E.R., and M.L.Y. conducted bioinformatic analyses. D.R. and M.H. pro-

vided patient samples. D.H. and J.H.K. designed and supervised the study. M.N., M.W.V., D.H., and J.H.K. crafted the manuscript. All authors revised and approved the manuscript.

Declaration of interests

J.H.K. has advisory roles for Bluebird Bio, Boehringer Ingelheim, Novartis, Roche and Jazz Pharmaceuticals. D.R. has advisory roles for Celgene Corporation, Novartis, Bluebird Bio, Janssen, and receives research funding from CLS Behring and Roche. M.H. receives research funding from Abbvie, Agios, Astellas, BergenBio, Bristol-Myers Squibb, Glycostem, Jazz Pharmaceuticals, Karyopharm, Loxo Oncology, and PinotBio, has received honoraria from Novartis, Pfizer, Jazz Pharmaceuticals, Janssen, Certara, and Sobi, and has advisory roles for Abbvie, BMS, Glycostem, Servier, PinotBio, Amgen, Pfizer, and LabDelbert.

Figure legends

Figure 1: CRISPRi screen of HSPC/AML IncRNA signatures.

See also Figures S1-2, Table S1.

- **a**, Expression of HSPC/AML IncRNAs across 12 normal blood cell populations and 46 pediatric AML samples⁶. Signatures of particular interest are outlined. Natural killer cell (NK), hematopoietic stem cell (HSC), common myeloid progenitor (CMP), granulocyte-monocyte progenitor (GMP), granulocyte (GC), monocyte (Mo), erythroid precursor (Ery), megakaryocyte (Mk), Down syndrome-associated myeloid leukemia (DS), non-DS megakaryoblastic leukemia (AMKL), promyelocytic leukemia (PML), *KMT2A*-rearranged leukemia (*KMT2A*-r).
- **b**, Conceptual workflow for screening HSPC/AML IncRNAs.
- **c**, Gene essentiality scores from pan-cell line MAGeCK analysis of the CRISPRi screen (6 cell lines, n=2 biological replicates each). The top hit *MYNRL15* is highlighted behind *MYC* and *MYB*, the positive controls. The top 10 hits are indicated on the right.
- **d**, Expression of *MYNRL15* compared to *bona fide* IncRNAs in the NCI-TARGET pediatric AML cohort (n=258). Midline, median; box limits, lower and upper quartiles; whiskers, 10% and 90% quantiles.
- **e**, Subcellular localization of MYNRL15 compared to controls XIST (nuclear), TERC (nuclear), and B2M (cytoplasmic), as determined via fractionated qRT-PCR (n=2 biological replicates, mean \pm s.e.m.).

Figure 2: Characterization of MYNRL15 as a myeloid leukemia dependency locus.

See also Figure S3.

- **a**, Schematic of the *MYNRL15* locus, including the target sites of the different perturbation constructs (not to scale). Target gene: *MYNRL15* (orange), *UNC45A* (black), *HDDC3* (grey), *UNC45A+HDDC3* (light grey). Perturbation strategy: CRISPRi (filled circle), gene excision (filled square), promoter excision (empty square), splice site disruption (empty triangle), RNAi (empty diamond), LNA-gapmeRs (empty triangle), CRISPR-Cas9 mediated knockout (filled triangle).
- **b**, Top: Endpoint depletion values from fluorescence-based proliferation assays that used CRISPRi to knock down MYNRL15 in different cell lines (same data as in Figure S1d; n=2 biological replicates, mean \pm s.e.m.). The data are normalized to day 0 and to the non-targeting control (sgLUC). Bottom: expression of MYNRL15 and its flanking coding genes after targeting the CRISPRi system to the MYNRL15 TSS, as determined via qRT-PCR (n=3 biological replicates, mean \pm s.e.m.; data normalized to the non-targeting control).
- **c**, Endpoint depletion values from fluorescence-based proliferation assays using different perturbation strategies to target *MYNRL15*, *UNC45A*, and/or *HDDC3*. Each point represents one vector used for perturbation (mean of n=3 biological replicates shown). The data are normalized to day 0 and to the non-targeting control.
- **d**, Fluorescence-based proliferation assays using MYNRL15 cDNAs to rescue the CRISPRi depletion phenotype (n=2 biological replicates, mean \pm s.e.m.; double positive sgRNA+cDNA cells are shown). **P<0.01 (two-tailed, unpaired t-test); all conditions share the same P-value. Colors denote sgRNA vectors, shapes denote cDNA vectors. Long isoform (L), short isoform (S).
- **c-d**, These experiments were performed in ML-2 cells.

Figure 3: Functional dissection of MYNRL15 locus reveals crucial regulatory regions.

See also Figure S4-5, Table S2.

- **a**, Tracks from the UCSC Genome Browser showing, from top to bottom: gene annotations, CpG islands, histone marks, and CTCF and cohesin occupancy (K562 ChIP-seq data from ENCODE).
- **b**, Tiling screen results using parallel CRISPRi (top) and CRISPR-Cas9 based (bottom) strategies to interrogate the *MYNRL15* locus shown in **a** (mean of 4 cell lines, n=2 biological replicates each). Previously tested sgRNAs are shown in color. A smoothed fit curve is shown in blue. The two cCREs, C1 and C2, are outlined. Positions are to scale to the annotation tracks shown above.
- **c**, Fluorescence-based proliferation assays using classical CRISPR-Cas9 and individual sgRNAs from C1 and C2 to achieve perturbation of the *MYNRL15* locus (n=3 biological replicates, mean ± s.e.m.; 2 guides per cCRE, 4 guides in total). The data are normalized to day 0 and to the non-targeting control (sgLUC). *P<0.05, **P<0.01, ****P<0.001 (two-tailed, unpaired t-tests); where only one set of asterisks is shown, all conditions share the same *P*-value.
- **d-g**, Differential expression analyses comparing the *MYNRL15* perturbation group (all 4 guides from **c**; "sgMYNRL15") to the non-targeting control ("sgLUC") in a combined analysis across early (day 3) and late (day 6 7, respectively) time points of ML-2 and K562 cells (n=2 biological replicates per guide).
- **d**, Volcano plot depicting differential gene expression following *MYNRL15* perturbation, as determined using DESeq2. The most significantly up- and downregulated genes are shown in pink and purple, respectively ($P_{adj} \le 10^{-5}$, |LFC| ≥ -0.5); chromosome 15 genes are shown in blue.
- **e**, Gene ontology terms enriched in the significantly up- (pink) and downregulated (purple) genes from **d**, as determined using the DAVID functional annotation tool. Erythroid (ery), intracellular (intracell), phosphorylation (phospho).
- f, Normalized enrichment scores (NES) of cancer dependency gene sets that are downregulated upon *MYNRL15* perturbation. Colors correspond to MSigDB collections H1 "hallmark" (turquoise) and C2 "KEGG pathways" (blue). ****P=0 (nominal P values from GSEA).
- **g**, Two chromosome 15 positional gene sets (1 Mb windows) that are downregulated upon *MYNRL15* perturbation, including a region around the *MYNRL15* locus (bottom). NES, *P*-values, and FDRs were calculated by GSEA.

Figure 4: MYNRL15 perturbation alters chromosome 15 conformation and expression of cancer dependency genes.

See also Figure S6, Tables S3-4.

- **a**, NG Capture-C interaction profiles on chromosome 15 in K562 and ML-2 cells, using one guide targeting *MYNRL15* (sgC1.1) and a non-targeting control (sgLUC) (n=2 biological replicates; viewpoint in C1; smoothing window 2 pixels).
- **b-c**, Close-ups of the gained distal interaction region and the region around *MYNRL15*, alongside K562 CTCF ChIP-Seq and H1-hESC Micro-C⁴⁷ tracks from the UCSC Genome Browser.
- **d**, Model of chromosome 15 reorganization following *MYNRL15* perturbation.
- **e**, Venn diagram depicting the 24 transcription factors that bind both C1 and C2, and whether they also bind the gained distal interaction regions (binding sites identified using ENCODE K562 ChIP-seq data).
- **f**, Integrative analysis of CRISPR-Cas9 screening scores (MAGeCK; n=2 per cell line) and differential expression after *MYNRL15* perturbation (DESeq2; comparison as in Figure 2d-e) for the 29 coding genes located in the gained distal interaction region. A combined analysis of K562 and ML-2 cells is shown.
- **g**, Left: integrative analysis of genome-wide CRISPR-Cas9 screening scores (DepMap K562 data) and differential expression after MYNRL15 perturbation (DESeq2; comparison as in Figure 2d-e). Downregulated dependency genes are shown in pink ($P_{adj} \le 10^{-3}$, CERES ≤ -0.5); chromosome 15 genes shown in blue. Right: gene ontology terms enriched in the downregulated dependency genes, as determined using the DAVID functional annotation tool.

Figure 5: Anti-leukemic effect of MYNRL15 perturbation in primary cells.

See also Figure S7, Table S5.

- **a**, Colony counts following *MYNRL15* perturbation in CD34⁺ HSPCs from healthy donors (n=3 biological replicates; mean ± s.e.m.). Replating capacity (left) and differentiation (right) were evaluated.
- **b**, Colony counts following *MYNRL15* perturbation in two patient-derived KMT2A-r pediatric AML samples (n=4 biological replicates; mean ± s.e.m.).
- **c**, Colony counts following *MYNRL15* perturbation in two AMKL and two ML-DS pediatric AML samples (n=2 biological replicates; mean ± s.e.m.).
- **d**, Colony counts following MYNRL15 perturbation in two normal karyotype adult AML samples (n=2 biological replicates; mean \pm s.e.m.).
- **e**, Comparison of *MYNRL15* perturbation in CD34⁺ HSPCs (n=3 biological replicates) versus 8 AML PDXs belonging to 4 subgroups (2 PDXs per subgroup): *KMT2A*-r (pediatric; n=4 biological replicates each), AMKL (pediatric; n=2), ML-DS (pediatric; n=2) and normal karyotype AML (adult; n=2). Data are normalized to the non-targeting control. Each dot represents a mean of replicates.
- **f**, Setup (left) and results (right) of direct two-color *in vivo* competition assays involving CRISPRi mediated perturbation of *MYNRL15* in AML PDXs. The data are presented as ratios of dTomato⁺ (dTom) to E2Crimson⁺ (E2C) cells in the bone marrow (bm), spleens (spl), and livers (li) of recipient mice (n=4 in the AML PDX #2 control group, otherwise n=5 per group; mean ± s.e.m.).
- **a-f**, *P* values were calculated using two-tailed, unpaired t-tests.

STAR Methods

Resource availability

Lead contact

Further information and requests for resources and reagents should be directed to and will be fulfilled by the lead contact, Jan-Henning Klusmann (jan-henning.klusmann@kgu.de).

Materials availability

All plasmids generated in this study have been deposited to Addgene. Plasmid catalog numbers are listed in the "lentiviral vectors" section of the Methods.

Data and code availability

RNA-seq and Capture-C data generated by this study have been deposited in the Gene Expression Omnibus (GEO) under the accession number GSE172240. Raw sequencing data from the CRISPR screens have been deposited in the European Nucleotide Archive (ENA) at EMBL-EBI under the accession numbers PRJEB44308 and PRJEB44320. Genome-wide CRISPR-Cas9 screening data were obtained from the DepMap Project²³ portal (https://depmap.org/portal/download). Histone and transcription factor ChIP-seq data from ENCODE, and Micro-C and Hi-C data from the 4D Nucleome Data Portal were used in this study (refer to Key Resources table for identifiers). RNA-seq data from adult and pediatric AML patients were obtained from TCGA (https://gdc.cancer.gov/access-data) and TARGET (https://gdc.cancer.gov/programs/target/data-matrix), respectively. Microarray data from normal hematopoietic cells and pediatric AML samples were previously generated by our lab⁶ (https://ag-klusmann.shinyapps.io/lncScape/).

This paper used existing analysis algorithms (see Methods) and does not report original code.

Any additional information required to reanalyze the data reported in this paper is available from the lead contacts upon request.

Experimental model and study participant details

Animal studies

This study involved animal experiments using NOD.Cg-Prkdc^{scid} Il2rgtm^{1Wji}/SzJ (NSG) immunodeficient mice (Charles River Laboratories). 8-10 week old female littermates were randomly assigned to experimental groups. The mice were group housed in individual ventilated cages with autoclaved food and water in a pathogen-free environment at the Martin Luther University Halle-Wittenberg. All animal procedures were approved by the state authorities (Landesverwaltungsamt Sachsen-Anhalt).

Human participants

Human CD34+ hematopoietic stem and progenitor cells (HSPCs) were isolated from mobilized peripheral blood of anonymous healthy donors. Acute myeloid leukemia (AML) samples were provided by the Berlin-Frankfurt-Münster Study Group (AML-BFM-SG, Essen Germany) and the Department of Hematology, Hemostasis, Oncology and Stem Cell Transplantation (Hannover Medical School). Informed consent was obtained from all human participants or custodians. Please refer to Table S5 for patient characteristics including sex and age. Information about gender was not collected, and patient characteristics were not provided for the anonymous healthy donors. All investigations were approved by the ethics committee of the Martin Luther University Halle-Wittenberg.

Cells and cell culture

HEK293T cells and the human leukemia cell lines K562, ML-2, M-07E, KASUMI-1, NOMO-1, SKNO-1, OCI-AML3, TF-1, NB-4 were obtained from the German National Resource Center for Biological Material (DSMZ, Braunschweig, Germany) and cultured according to their recommendations. The cells were authenticated by the vendor and no further authentication was performed in the laboratory. All cell lines were routinely tested for mycoplasma contamination. Cell line characteristics including sex and age can be found in Table S5. Culture conditions for primary HSPCs and patient-derived AML cells are described in the "hemato-poietic assays" section of the Methods.

Method details

Lentiviral vectors

Individual single guide RNAs (sgRNAs) were designed using CCTop⁴⁸ (https://cctop.cos.uni-heidelberg.de/), and cloned via BsmBI into the SGL40C.EFS.dTomato (Addgene 89395) or SGL40C.EFS.E2Crimson (100894) backbone. Dual sgRNA vectors were generated by cloning a second promoter (mU6)-sgRNA cassette (207866) into an existing (hU6) sgRNA vector via EcoRI/XhoI. Short hairpin RNAs (shRNAs) for RNA interference were designed using the Adams *et al.* miR-N tool⁴⁹ (https://felixfadams.shinyapps.io/miRN/) and cloned via BsmBI into the SIN40C.SFFV.eGFP.miR30n (169278) backbone. Non-targeting sgRNAs and shRNAs were designed against firefly luciferase. *MYNRL15* cDNAs were expressed from the bidirectional LBid.Inc.GFP^{50,51} vector. The L40C-CRISPR.EFS.mNeon (69146) all-in-one system was used on primary cells for *in vitro* hematopoietic assays. Stable cell lines were generated using pLKO5d.SFFV.dCas9-KRAB.P2A.BSD (90332) or pLKO5d.EFS.SpCas9.P2A.BSD (57821). Stable patient-derived xenografts were made using SIN40C.SFFV.dCas9-KRAB.P2A.mNeon (170482). The sgRNA libraries used in this study were expressed from SGL40C.EFS.dTomato (89395; CRISPRi IncRNA and *MYNRL15* tiling) and SGL.EFS.tBFP (173915; gained chromatin interaction region).

Individual sgRNA and shRNA sequences are listed in Table S6. The sgRNA sequences of the three CRISPR libraries in this study are provided in Tables S1, S2, and S4.

Lentiviruses

Lentiviral particles were produced by co-transfecting the expression vector and the packaging plasmids pMD2.G and psPAX2 (Addgene 12259 and 12260 respectively) into HEK293T cells using polyethylenimine (PEI). Viral particles were concentrated via ultracentrifugation, and in the case of all-in-one constructs, were further concentrated using Lenti-X™ Concentrator reagent (TaKaRa). Transductions were performed in normal cell culture media, in the presence of Polybrene (Sigma-Aldrich).

LNA-GapmeRs

Custom- antisense LNA-GapmeRs targeting the *MYNRL15* transcript were obtained from Qiagen through their in-house design tool. Negative control B (Qiagen 339515) was used as a non-targeting control. Cells were cultured in media containing 2.5 µM LNA-GapmeR for delivery by unassisted uptake⁵². Fresh LNA-GapmeR was added every 2 days to maintain its concentration in the culture media. LNA-GapmeR sequences can be found in Table S6.

CRISPR library design

Guides for CRISPRi-based targeting of HSPC/AML IncRNAs were designed using the standalone version of CCTop⁴⁸ (https://cctop.cos.uni-heidelberg.de/). In brief, IncRNA genes were annotated using GENCODE v25 (release 03/2016)⁵³, LNCipedia 4.0 (release 05/2016)⁵⁴, and NONCODE v4 (release 01/2014)⁵⁵ as previously described⁶, and sgRNAs were selected 0-250 bp downstream of transcription start sites (TSSs)⁵⁶. Three to nine sgRNAs were selected per gene, depending on the number of different TSSs present in the transcript isoforms and the distance between them. Genes with a single TSS, or with multiple TSSs with high transcript-level support (TSL 1 or 2, according to Ensembl annotations) spaced more than 300 bp apart, were targeted using three sgRNAs per TSS in a 0-150 bp window downstream of the respective TSS. Genes with multiple TSSs in close proximity to each other (spaced ≤150 bp apart) were targeted using five sgRNAs in a 0-250 bp window downstream of the first TSS. Guides were prioritized for low off-target binding – a criterion that is built-in to the CCTop tool.

Guides tiling the *MYNRL15* locus were designed by inputting 15 kb of DNA sequence (hg38) symmetrically centered on *MYNRL15* into the CRISPOR⁵⁷ (http://crispor.tefor.net/) saturating mutagenesis assistant. To maintain dense tiling of the region (mean coverage: 0.11 sgRNAs per bp), only guides with an MIT specificity score of 0 were excluded.

Guides targeting the 29 protein-coding genes located in the gained distal chromatin interaction region were designed using CCTop⁴⁸ (https://cctop.cos.uni-heidelberg.de/). Coding regions (CDS) from Ensembl v102 (release 11/2020) were used as inputs, and where possi-

ble, sgRNAs were selected to target most, if not all, protein-coding isoforms. Guides were prioritized for low off-target binding, and those with low predicted on-target efficacies (CRIS-PRater⁵⁸ score<0.4) were excluded.

Due to our usage of SGL40C vectors for lentiviral sgRNA delivery, in which sgRNA transcription is driven from a human U6 promoter, guides containing poly-T stretches (4 or more) were excluded from all libraries, to avoid premature termination of sgRNA transcription mediated by RNA polymerase III. Guides directed against luciferase and the neomycin resistance cassette were used as non-targeting controls, guides targeting *PPP1R12C* and *SLC22A13* were used as nonessential cutting controls, and guides against *MYC*, *MYB*, *ACTB*, *U2AF1*, *RPL9*, and *POL2RA* were used as positive depletion controls. The sgRNA spacer sequences of the three CRISPR libraries used in this study are provided in Tables S1, S2, and S4.

CRISPR library cloning and screening

Library spacer sequences were purchased from Integrated DNA Technologies, pooled, and cloned via BsmBI into one of the following vectors: SGL40C.EFS.dTomato (Addgene 89395; CRISPRi IncRNA and *MYNRL15* tiling), and SGL.EFS.tBFP (173915; gained chromatin interaction region). XL1-Blue supercompetent cells (Agilent 200236) were used for transformation, and subsequently plated on 15 cm LB agar plates containing ampicillin. Colonies were counted from 1 cm² areas to ensure sufficient library representation, and then harvested and prepped for plasmid DNA using the QIAGEN Plasmid Maxi Kit. Lentiviral particles were produced as outlined above.

Stable dCas9-KRAB- or Cas9-expressing cell lines were transduced with the sgRNA libraries at an MOI of 0.3, and maintained at 1000-fold representation of the library for 16-18 population doublings. The screens were counted every 2-3 days and split accordingly. Samples were taken at the beginning and end of the screen, to determine differences in sgRNA abundance over time and thereby identify essential genes or regions. Genomic DNA was isolated from these samples via the QIAmp DNA Blood Mini Kit (Qiagen), and the sgRNA

cassettes were PCR amplified using the NEBNext® High-Fidelity 2x PCR Master Mix (New England Biolabs) and barcoded primers containing the Illumina P5 and P7 adapter sequences as overhangs. The sgRNA amplicons (~300 bp) were gel purified using the GeneJET Gel Extraction Kit (Thermo Fisher Scientific) and sequenced on an Illumina HiSeq 2000 (50 bp single-end reads).

We applied the MAGeCK (<u>m</u>odel-based <u>a</u>nalysis of <u>g</u>enome-wide <u>C</u>RISPR-Cas9 <u>k</u>nockout)¹⁸ pipeline to process raw reads and call AML dependency genes from the CRISPRi IncRNA and gained chromatin interaction region screens. The *MYNRL15* tiling screens were analysed in R using DESeq2⁵⁹ (Bioconductor).

Fluorescence-based proliferation assays

Individual proliferation assays were conducted in stable dCas9-KRAB- or Cas9-expressing cell lines for CRISPR/Cas9 experiments, and in wild-type lines for RNAi experiments. Cells were transduced with individual sgRNA or shRNA perturbation constructs at an efficiency of 40-80%, to attain a mixed population allowing for direct competition between transduced and untransduced cells. These cultures were maintained for up to 20 days, during which fluorescence was tracked every 2-3 days via flow cytometry. Depletion curves were generated by normalizing the percentage of fluorescent (i.e. transduced) cells at each time point to both the initial fluorescence (day 0) and the non-targeting control (sgLUC / shLUC). For the rescue experiment with *MYNRL15* cDNAs, sgRNA-expressing cells were transduced a second time with the cDNA expression constructs. The double-positive population was then tracked by flow cytometry.

Flow cytometry and cell sorting

Flow cytometry data were collected on a CytoFLEX B4-R3-V5 or CytoFLEX S V4-B2-Y4-R3 using CytExpert software (Beckman Coulter). Cell sorting was performed on a FACSAria™ II using FACSDiva™ software, or on a FACSMelody™ using FACSChorus™ software (BD Biosciences). An anti-human CD45 FITC (Beckman Coulter) antibody was used to analyze

xenotransplantation experiments. Kaluza 2.1 (Beckman Coulter) or FlowJo™ v10.6 (BD Biosciences) software was used for data analysis.

Hematopoietic assays

CD34⁺ HSPCs were thawed and expanded in StemSpan SFEM (STEMCELL Technologies) containing 1% penicillin/streptomycin (Gibco[™]), 100 ng/ml SCF, 100 ng/ml FLT3L, 20 ng/ml IL6, 50 ng/ml TPO (cytokines from Peprotech), and 750nM SR1 (STEMCELL Technologies) for 2 days prior to transduction. Cells were transduced in the presence of 4 µg/ml Polybrene (Sigma-Aldrich) on RetroNectin®-coated plates (TaKaRa), using two consecutive rounds of super-concentrated virus. Four days post-transduction, the cells were sorted and plated in human methylcellulose complete medium HSC003 (R&D Systems) for colony-forming assays. Fifteen thousand cells were initially plated over two 6 mm dishes. The colonies were counted once they had reached a sufficient size (10-14 days).

For assays using patient-derived AML blasts, *in vivo* expanded samples were thawed and pre-cultured in StemSpan SFEM (STEMCELL Technologies) containing 1% penicil-lin/streptomycin (GibcoTM), 50 ng/ml SCF, 50 ng/ml FLT3L, 10 ng/ml IL6, 2.5 ng/ml IL3, 10 ng/ml TPO (cytokines from Peprotech), and 750 nM SR1 and 35 nM UM171 (both from STEMCELL Technologies) for 24-48 hours. Transductions were conducted in the presence of 2 μg/ml Polybrene (Sigma-Aldrich). The cells were harvested 48 hours post-transduction for xenotransplantation into mice or for colony-forming assays.

Animal experiments

Two-color *in vivo* competition experiments were performed in murine xenograft models of AML as previously described^{50,60}. In brief, stable dCas9-KRAB cell lines or *in vivo* expanded patient-derived AML cells (PDXs) were transduced with E2Crimson or dTomato sgRNA vectors, mixed 1:1, and injected via tail vein into irradiated (2.5 Gy), 8-10 week old NOD.Cg-Prkdc^{scid} Il2rgtm^{1Wjl}/SzJ (NSG) recipients. One to two million cells were injected per mouse, and tracked via flow cytometry on peripheral blood samples every 4 weeks. The mice were sacrificed upon leukemia onset, at which point cells were isolated from the bone marrow,

spleen, and liver, and analyzed by flow cytometry. An anti-human CD45 antibody was used to track AML cell lines, which were generated using the dCas9-KRAB.P2A.BSD construct (Addgene 90332). The PDXs were generated using the dCas9-KRAB.P2A.mNeon construct (170482); thus, fluorescence-based tracking was sufficient. sgRNA-containing E2Crimson or dTomato cell populations were compared to determine relative proliferation. All mice were housed under a 12 hour light / 12 hour dark cycle in a pathogen-free environment at the Martin Luther University Halle-Wittenberg. All animal procedures were approved by the local state authorities (Landesverwaltungsamt Sachsen-Anhalt).

RNA sequencing

RNA was isolated from cells using the Quick-RNATM Miniprep Kit (Zymo Research) on days 3 and 6 or 7 post-transduction (for ML-2 and K562, respectively; the late time point was selected based on depletion kinetics in Figure 2c). PolyA-enriched total cellular RNA sequencing was performed by Novogene Company, Ltd. on an Illumina NovaSeq 6000 using 150 bp paired-end chemistry. The raw sequence data were processed by Novogene using a standard pipeline. In brief, reads were filtered using in-house scripts and mapped to human reference genome hg38 using HISAT2⁶¹, and gene expression was quantified using the feature-Counts⁶² function in R. Differential expression analysis was conducted in R using DESeq2⁵⁹ (Bioconductor). Gene sets from MSigDB v7.2 (H1, C2, C3, C6), custom hematopoietic⁶ and chromosome 15 gene sets, and PAF1c-knockout expression signatures²⁷ were tested for enrichment using the Broad GSEA software⁶³. Custom positional gene sets were generated by walking a 1 Mb or 5 Mb window along chromosome 15. Gene ontology analysis was carried out using the DAVID⁶⁴ functional annotation tool (https://david.ncifcrf.gov/summary.jsp).

NG Capture-C

Chromatin conformation capture with selective enrichment for *MYNRL15*-interacting sequences was performed using next generation (NG) Capture-C as previously described²², with minor modifications: (1) 5-10 million cells were harvested per sample and DpnII digestion reactions were scaled down accordingly. (2) DNA was sheared to 200 bp using a Bran-

son 450 Digital Sonifier (Marshall Scientific) (time 18 s, amplitude 20%, pulse 0.5 s, pause 1.5 s; repeat 5x). (3) All of the material from the first capture was used as input for the second capture. (4) The libraries were sequenced by Novogene Company, Ltd. on an Illumina NovaSeq 6000 (150 bp paired-end reads). sgRNA-transduced K562 and ML-2 cells (day 3 post-transduction) and *in vitro* expanded CD34+ HSPCs (day 3 post-thawing) were used to evaluate the effect of *MYNRL15* perturbation and the normal conformation of the locus, respectively. We used biotinylated oligonucleotides (sequences in Table S6) targeting a viewpoint in the candidate *cis*-regulatory region C1 to enrich for interactions involving the locus. Two biological replicates were prepared per sample and pooled prior to oligonucleotide capture.

The biotinylated capture oligonucleotides designed using CapSegum2⁶⁵ were (https://capsegum.molbiol.ox.ac.uk/cgi-bin/CapSegum.cgi) and purchased from Integrated DNA Technologies. Raw sequence data were processed with the capC-MAP package⁶⁶ using default settings. Normalized pileups (RPMs; binstep=3000, window=6000) were capped at the 99th percentile and scaled to the maximum signal within the sample, so that crosssample comparisons could be made on a 0-1 scale. The data were visualized in the UCSC Genome Browser⁶⁷ using a smoothing window of 2 pixels, alongside CTCF ChIP-seq data from K562 cells (ENCODE accession no. ENCFF519CXF) and Knight-Ruiz matrixbalanced⁶⁸ Micro-C⁶⁹ data from H1-hESC cells. Hi-C data from Rao et al.⁷⁰ were also used to confirm the presence of specific 3D chromatin structures in other cell lines.

Dual luciferase assays

Dual luciferase assays were performed using the Dual-Luciferase® Reporter Assay System (Promega). The candidate *cis*-regulatory regions C1 and C2 were cloned alone or in combination upstream of the minimal promoter in the pGL4.23 firefly luciferase reporter construct (Promega E8411). A pGL4.7 *Renilla* luciferase reporter construct (Promega E6881) driven from the EF1α promoter was used as a background control. The firefly and *Renilla* vectors were co-transfected into K562 cells at a 20:1 ratio via nucleoporation, using the Lonza 4D-

Nucleofector[™] and SF Cell Line X Kit S. 24 h post-transfection, cells were harvested and measured on a GloMax® 96 Luminometer (Promega).

Quantitative real-time PCR

RNA was isolated from cells using the Quick-RNA[™] Microprep or Miniprep Kits (Zymo Research), between days 3 to 5 post-transduction. RNA fractionation was performed as previously described⁷¹, except that we directly lysed the nuclear pellet instead of isolating the nuclear-soluble and chromatin-associated fractions separately. *B2M* and *XIST* were utilized as cytoplasmic and nuclear controls, respectively. The TURBO DNA-freeTM Kit (Invitrogen) was used for DNase treatment. Total cDNA was synthesized using the High-Capacity cDNA Reverse Transcription Kit, and gene expression was quantified by real-time PCR using SYBRTM Select Master Mix and gene-specific primers on a StepOnePlusTM Real-Time PCR cycler (all products from Applied Biosystems). *B2M* was used as a housekeeping control. Primers for qRT-PCR can be found in Table S6. QuantiTect® primer assays were used to detect *WDR61* and *IMP3* (Qiagen QT00083776 and QT00232330).

CRISPR-Cas9 indel and excision validation

PCR-based methods were used to validate CRISPR-Cas9 mediated insertions and deletions (indels; to knock out protein-coding genes) and *MYNRL15* excision via paired sgRNAs. Cells were harvested between days 3 and 5 post-transduction, and genomic DNA was isolated using the Quick-DNATM Miniprep Kit (Zymo Research). We relied on TIDE⁷² (tracking of indels by decomposition) to assess knockout efficiency; thus, we PCR amplified ~700 bp genomic regions centered on the corresponding sgRNA target sites from knockout and control (wild type) samples. The resulting products were subjected to Sanger sequencing, and knockout and wild type sequences were compared in the TIDE⁷² online tool (http://shinyapps.datacurators.nl/tide/). To validate *MYNRL15* excision, we performed PCR using primers flanking the region to be excised, thereby allowing us to ascertain deletion based on the size of the PCR product. All PCR primer sequences can be found in Table S6.

TCGA / TARGET

RNA-seq data from adult and pediatric AML patient cohorts were obtained from TCGA⁷³ (https://gdc.cancer.gov/access-data) and TARGET⁷⁴ (https://ocg.cancer.gov/programs/target/data-matrix), respectively. DESeq2 (Bioconductor) was used to normalize and variance-stabilize read count data⁵⁹. The TARGET dataset also required batch correction, for which we used sva⁷⁵ (Bioconductor). Normalized (and batch corrected) expression values were used for subsequent analyses. Unsupervised clustering was performed using Rtsne⁷⁶ (base R).

Quantifications and statistical analysis

Statistical evaluations of experimental data were carried out in GraphPad Prism 9 using two-tailed, unpaired t tests. Data are presented as mean \pm s.d. or s.e.m. as indicated in the figure legends. Statistical analyses of gene expression data (RNA-seq) were carried out in R using DESeq2⁵⁹, or via the Broad GSEA software⁶³. CRISPR-Cas9 screening data were analyzed using MAGeCK¹⁸ to call essential genes, with the exception of the tiling screens, which were analyzed in R using DESeq2. Differences with P<0.05 were considered significant. Sample sizes are indicated in the figure legends. No statistical methods were used to predetermine sample size.

Supplemental tables

Table S1: CRISPRi IncRNA library and screening results. Related to Figure 1.

Table S2: MYNRL15 tiling library and screening results. Related to Figure 3.

Table S3: Transcription factor binding analysis. Related to Figure 4.

Table S4: Capture-C gained region library and screening results. Related to Figure 4.

Table S5: Patient sample and AML cell line characteristics. Related to Figure 5.

Table S6: Sequences of individual oligonucleotides. Related to Figures 2-5.

References

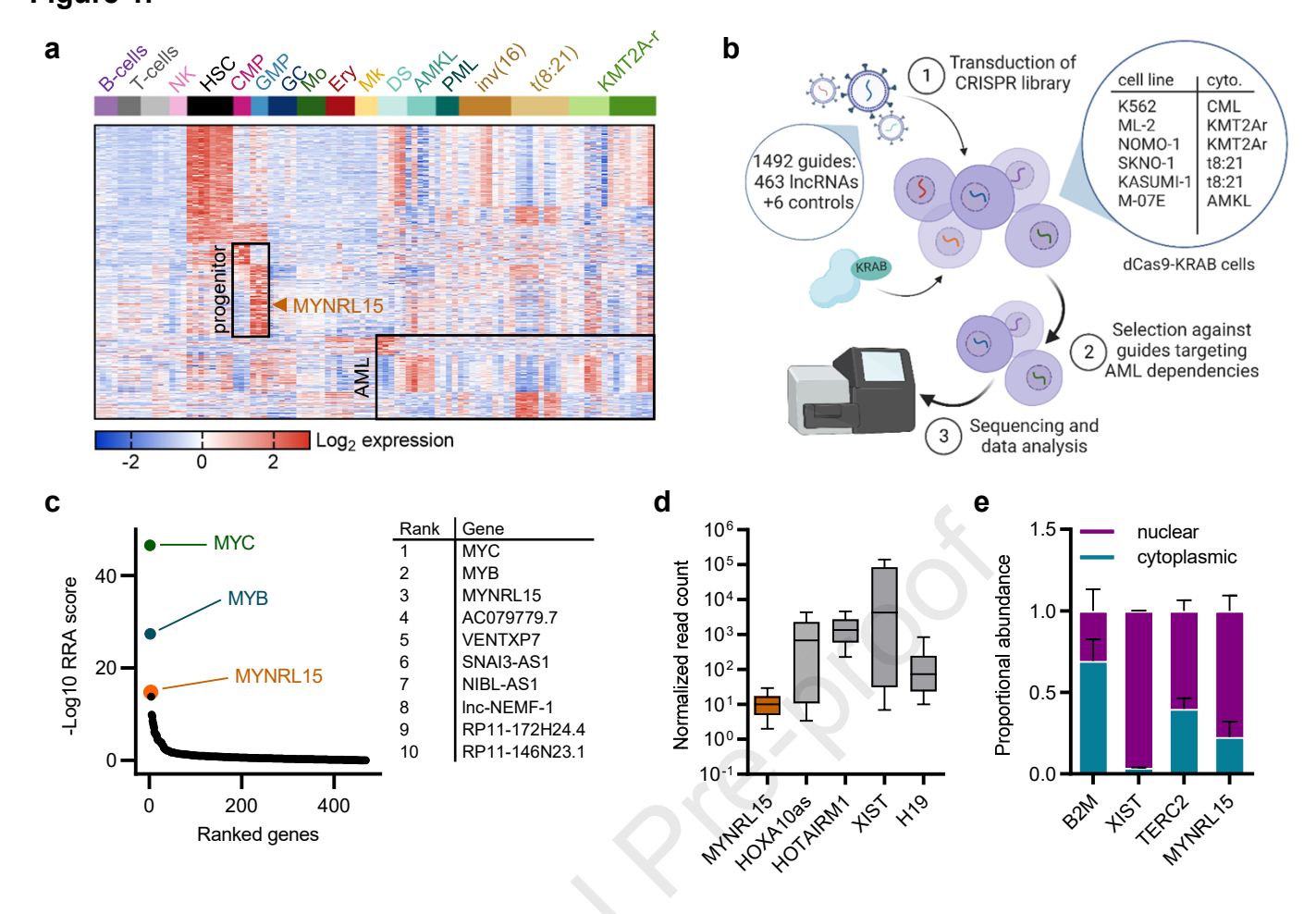
- 1. Consortium, E.P., Moore, J.E., Purcaro, M.J., Pratt, H.E., Epstein, C.B., Shoresh, N., Adrian, J., Kawli, T., Davis, C.A., Dobin, A., et al. (2020). Expanded encyclopaedias of DNA elements in the human and mouse genomes. Nature *583*, 699-710. 10.1038/s41586-020-2493-4.
- 2. Slack, F.J., and Chinnaiyan, A.M. (2019). The Role of Non-coding RNAs in Oncology. Cell 179, 1033-1055. 10.1016/j.cell.2019.10.017.
- 3. Zhou, S., Treloar, A.E., and Lupien, M. (2016). Emergence of the Noncoding Cancer Genome: A Target of Genetic and Epigenetic Alterations. Cancer Discov *6*, 1215-1229. 10.1158/2159-8290.CD-16-0745.
- 4. Short, N.J., Rytting, M.E., and Cortes, J.E. (2018). Acute myeloid leukaemia. Lancet *392*, 593-606. 10.1016/S0140-6736(18)31041-9.
- 5. Garzon, R., Volinia, S., Papaioannou, D., Nicolet, D., Kohlschmidt, J., Yan, P.S., Mrozek, K., Bucci, D., Carroll, A.J., Baer, M.R., et al. (2014). Expression and prognostic impact of IncRNAs in acute myeloid leukemia. Proc Natl Acad Sci U S A *111*, 18679-18684. 10.1073/pnas.1422050112.
- 6. Schwarzer, A., Emmrich, S., Schmidt, F., Beck, D., Ng, M., Reimer, C., Adams, F.F., Grasedieck, S., Witte, D., Kabler, S., et al. (2017). The non-coding RNA landscape of human hematopoiesis and leukemia. Nat Commun *8*, 218. 10.1038/s41467-017-00212-4.
- 7. Beck, D., Thoms, J.A.I., Palu, C., Herold, T., Shah, A., Olivier, J., Boelen, L., Huang, Y., Chacon, D., Brown, A., et al. (2018). A four-gene LincRNA expression signature predicts risk in multiple cohorts of acute myeloid leukemia patients. Leukemia *32*, 263-272. 10.1038/leu.2017.210.
- 8. Bill, M., Papaioannou, D., Karunasiri, M., Kohlschmidt, J., Pepe, F., Walker, C.J., Walker, A.E., Brannan, Z., Pathmanathan, A., Zhang, X., et al. (2019). Expression and functional relevance of long non-coding RNAs in acute myeloid leukemia stem cells. Leukemia 33, 2169-2182. 10.1038/s41375-019-0429-5.
- 9. Kopp, F., and Mendell, J.T. (2018). Functional Classification and Experimental Dissection of Long Noncoding RNAs. Cell *172*, 393-407. 10.1016/j.cell.2018.01.011.
- 10. Ng, M., Heckl, D., and Klusmann, J.H. (2019). The Regulatory Roles of Long Noncoding RNAs in Acute Myeloid Leukemia. Front Oncol *9*, 570. 10.3389/fonc.2019.00570.
- 11. Papaioannou, D., Petri, A., Dovey, O.M., Terreri, S., Wang, E., Collins, F.A., Woodward, L.A., Walker, A.E., Nicolet, D., Pepe, F., et al. (2019). The long non-coding RNA HOXB-AS3 regulates ribosomal RNA transcription in NPM1-mutated acute myeloid leukemia. Nat Commun *10*, 5351. 10.1038/s41467-019-13259-2.
- 12. Zhu, G., Luo, H., Feng, Y., Guryanova, O.A., Xu, J., Chen, S., Lai, Q., Sharma, A., Xu, B., Zhao, Z., et al. (2021). HOXBLINC long non-coding RNA activation promotes leukemogenesis in NPM1-mutant acute myeloid leukemia. Nat Commun *12*, 1956. 10.1038/s41467-021-22095-2.
- 13. Luo, H., Zhu, G., Eshelman, M.A., Fung, T.K., Lai, Q., Wang, F., Zeisig, B.B., Lesperance, J., Ma, X., Chen, S., et al. (2022). HOTTIP-dependent R-loop formation regulates CTCF boundary activity and TAD integrity in leukemia. Mol Cell *82*, 833-851 e811. 10.1016/j.molcel.2022.01.014.
- 14. Sartorelli, V., and Lauberth, S.M. (2020). Enhancer RNAs are an important regulatory layer of the epigenome. Nat Struct Mol Biol *27*, 521-528. 10.1038/s41594-020-0446-0.
- 15. Cho, S.W., Xu, J., Sun, R., Mumbach, M.R., Carter, A.C., Chen, Y.G., Yost, K.E., Kim, J., He, J., Nevins, S.A., et al. (2018). Promoter of lncRNA Gene PVT1 Is a Tumor-Suppressor DNA Boundary Element. Cell *173*, 1398-1412 e1322. 10.1016/j.cell.2018.03.068.
- 16. Eppert, K., Takenaka, K., Lechman, E.R., Waldron, L., Nilsson, B., van Galen, P., Metzeler, K.H., Poeppl, A., Ling, V., Beyene, J., et al. (2011). Stem cell gene expression programs influence clinical outcome in human leukemia. Nat Med *17*, 1086-1093. 10.1038/nm.2415.

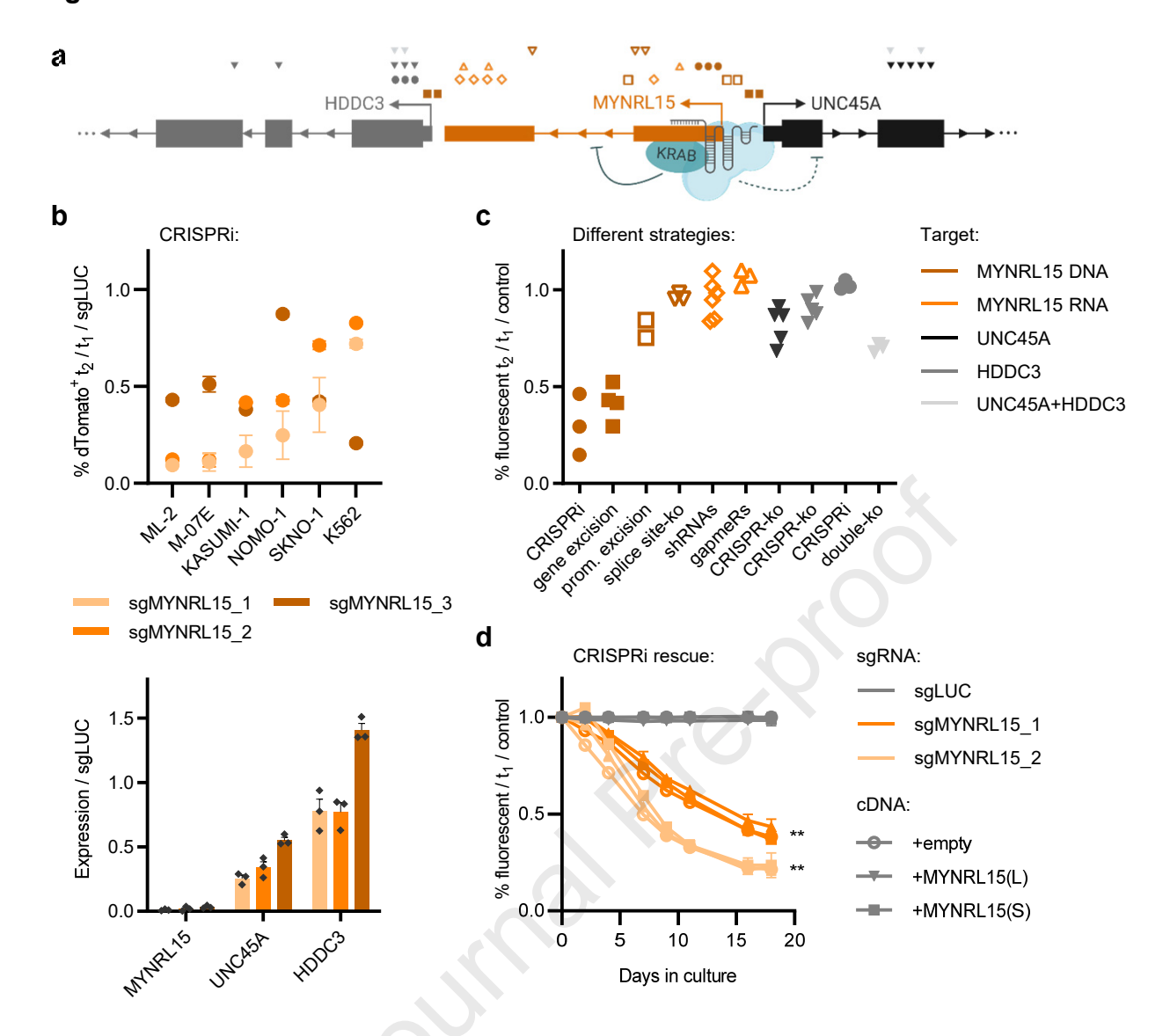
- 17. Krivtsov, A.V., Figueroa, M.E., Sinha, A.U., Stubbs, M.C., Feng, Z., Valk, P.J., Delwel, R., Dohner, K., Bullinger, L., Kung, A.L., et al. (2013). Cell of origin determines clinically relevant subtypes of MLL-rearranged AML. Leukemia *27*, 852-860. 10.1038/leu.2012.363.
- 18. Li, W., Xu, H., Xiao, T., Cong, L., Love, M.I., Zhang, F., Irizarry, R.A., Liu, J.S., Brown, M., and Liu, X.S. (2014). MAGeCK enables robust identification of essential genes from genomescale CRISPR/Cas9 knockout screens. Genome Biol *15*, 554. 10.1186/s13059-014-0554-4.
- 19. Liu, S.J., Horlbeck, M.A., Cho, S.W., Birk, H.S., Malatesta, M., He, D., Attenello, F.J., Villalta, J.E., Cho, M.Y., Chen, Y., et al. (2017). CRISPRi-based genome-scale identification of functional long noncoding RNA loci in human cells. Science *355*. 10.1126/science.aah7111.
- 20. Liu, Y., Cao, Z., Wang, Y., Guo, Y., Xu, P., Yuan, P., Liu, Z., He, Y., and Wei, W. (2018). Genome-wide screening for functional long noncoding RNAs in human cells by Cas9 targeting of splice sites. Nat Biotechnol. 10.1038/nbt.4283.
- 21. Joung, J., Engreitz, J.M., Konermann, S., Abudayyeh, O.O., Verdine, V.K., Aguet, F., Gootenberg, J.S., Sanjana, N.E., Wright, J.B., Fulco, C.P., et al. (2017). Genome-scale activation screen identifies a lncRNA locus regulating a gene neighbourhood. Nature *548*, 343-346. 10.1038/nature23451.
- 22. Davies, J.O., Telenius, J.M., McGowan, S.J., Roberts, N.A., Taylor, S., Higgs, D.R., and Hughes, J.R. (2016). Multiplexed analysis of chromosome conformation at vastly improved sensitivity. Nat Methods *13*, 74-80. 10.1038/nmeth.3664.
- 23. Tsherniak, A., Vazquez, F., Montgomery, P.G., Weir, B.A., Kryukov, G., Cowley, G.S., Gill, S., Harrington, W.F., Pantel, S., Krill-Burger, J.M., et al. (2017). Defining a Cancer Dependency Map. Cell *170*, 564-576 e516. 10.1016/j.cell.2017.06.010.
- 24. Granneman, S., Gallagher, J.E., Vogelzangs, J., Horstman, W., van Venrooij, W.J., Baserga, S.J., and Pruijn, G.J. (2003). The human Imp3 and Imp4 proteins form a ternary complex with hMpp10, which only interacts with the U3 snoRNA in 60-80S ribonucleoprotein complexes. Nucleic Acids Res *31*, 1877-1887. 10.1093/nar/gkg300.
- 25. Milne, T.A., Kim, J., Wang, G.G., Stadler, S.C., Basrur, V., Whitcomb, S.J., Wang, Z., Ruthenburg, A.J., Elenitoba-Johnson, K.S., Roeder, R.G., and Allis, C.D. (2010). Multiple interactions recruit MLL1 and MLL1 fusion proteins to the HOXA9 locus in leukemogenesis. Mol Cell *38*, 853-863. 10.1016/j.molcel.2010.05.011.
- 26. Muntean, A.G., Tan, J., Sitwala, K., Huang, Y., Bronstein, J., Connelly, J.A., Basrur, V., Elenitoba-Johnson, K.S., and Hess, J.L. (2010). The PAF complex synergizes with MLL fusion proteins at HOX loci to promote leukemogenesis. Cancer Cell *17*, 609-621. 10.1016/j.ccr.2010.04.012.
- Saha, N., Ropa, J., Chen, L., Hu, H., Mysliwski, M., Friedman, A., Maillard, I., and Muntean, A.G. (2019). The PAF1c Subunit CDC73 Is Required for Mouse Hematopoietic Stem Cell Maintenance but Displays Leukemia-Specific Gene Regulation. Stem Cell Reports 12, 1069-1083. 10.1016/j.stemcr.2019.03.010.
- 28. Lupianez, D.G., Kraft, K., Heinrich, V., Krawitz, P., Brancati, F., Klopocki, E., Horn, D., Kayserili, H., Opitz, J.M., Laxova, R., et al. (2015). Disruptions of topological chromatin domains cause pathogenic rewiring of gene-enhancer interactions. Cell *161*, 1012-1025. 10.1016/j.cell.2015.04.004.
- 29. Despang, A., Schopflin, R., Franke, M., Ali, S., Jerkovic, I., Paliou, C., Chan, W.L., Timmermann, B., Wittler, L., Vingron, M., et al. (2019). Functional dissection of the Sox9-Kcnj2 locus identifies nonessential and instructive roles of TAD architecture. Nat Genet *51*, 1263-1271. 10.1038/s41588-019-0466-z.
- 30. Flavahan, W.A., Drier, Y., Liau, B.B., Gillespie, S.M., Venteicher, A.S., Stemmer-Rachamimov, A.O., Suva, M.L., and Bernstein, B.E. (2016). Insulator dysfunction and oncogene activation in IDH mutant gliomas. Nature *529*, 110-114. 10.1038/nature16490.
- 31. Schoenfelder, S., and Fraser, P. (2019). Long-range enhancer-promoter contacts in gene expression control. Nat Rev Genet *20*, 437-455. 10.1038/s41576-019-0128-0.

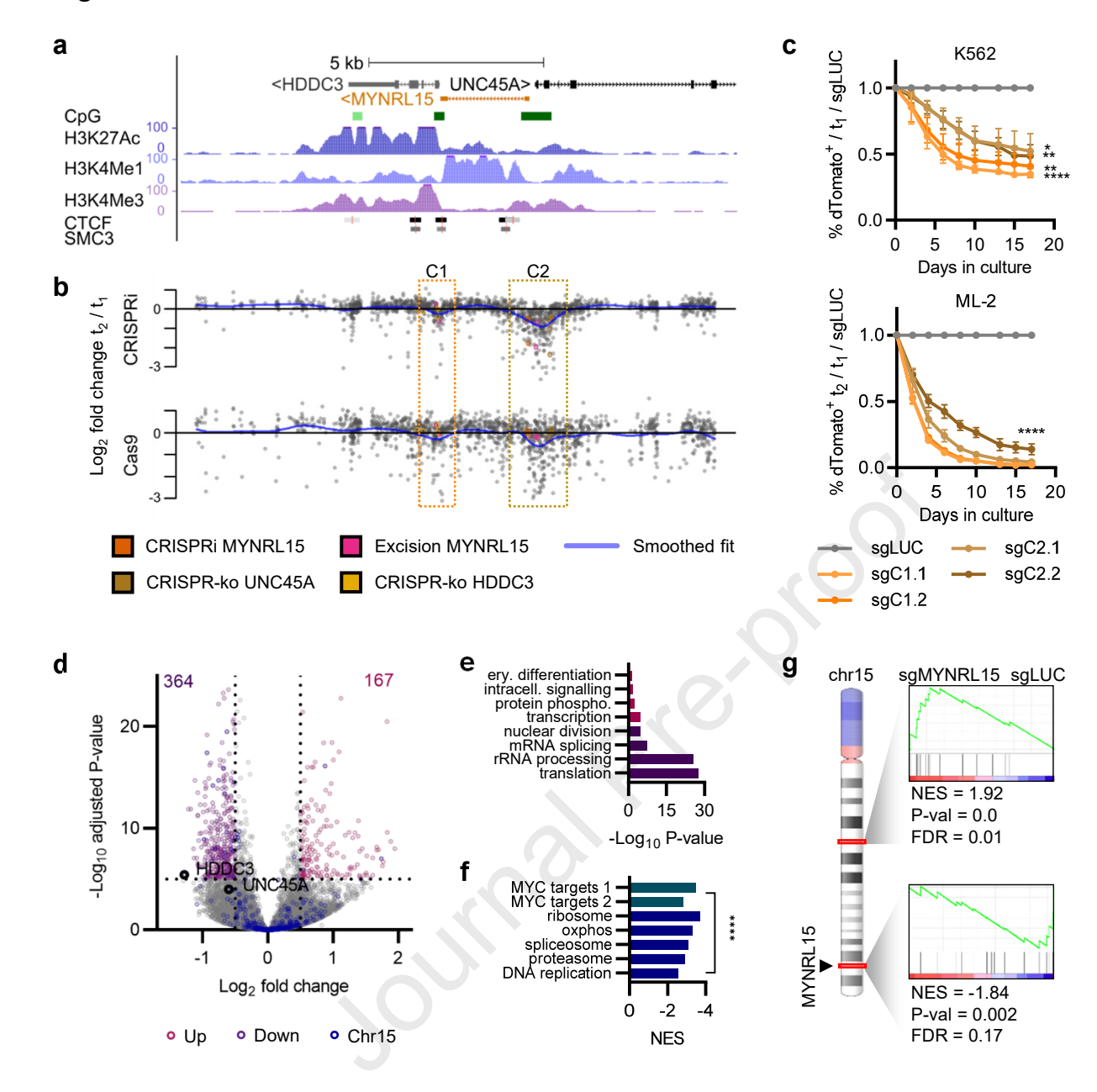
- 32. Hnisz, D., Weintraub, A.S., Day, D.S., Valton, A.L., Bak, R.O., Li, C.H., Goldmann, J., Lajoie, B.R., Fan, Z.P., Sigova, A.A., et al. (2016). Activation of proto-oncogenes by disruption of chromosome neighborhoods. Science *351*, 1454-1458. 10.1126/science.aad9024.
- 33. Akdemir, K.C., Le, V.T., Chandran, S., Li, Y., Verhaak, R.G., Beroukhim, R., Campbell, P.J., Chin, L., Dixon, J.R., Futreal, P.A., et al. (2020). Disruption of chromatin folding domains by somatic genomic rearrangements in human cancer. Nat Genet *52*, 294-305. 10.1038/s41588-019-0564-y.
- 34. Katainen, R., Dave, K., Pitkanen, E., Palin, K., Kivioja, T., Valimaki, N., Gylfe, A.E., Ristolainen, H., Hanninen, U.A., Cajuso, T., et al. (2015). CTCF/cohesin-binding sites are frequently mutated in cancer. Nat Genet *47*, 818-821. 10.1038/ng.3335.
- 35. Groschel, S., Sanders, M.A., Hoogenboezem, R., de Wit, E., Bouwman, B.A.M., Erpelinck, C., van der Velden, V.H.J., Havermans, M., Avellino, R., van Lom, K., et al. (2014). A single oncogenic enhancer rearrangement causes concomitant EVI1 and GATA2 deregulation in leukemia. Cell *157*, 369-381. 10.1016/j.cell.2014.02.019.
- 36. Jung, N., Dai, B., Gentles, A.J., Majeti, R., and Feinberg, A.P. (2015). An LSC epigenetic signature is largely mutation independent and implicates the HOXA cluster in AML pathogenesis. Nat Commun *6*, 8489. 10.1038/ncomms9489.
- 37. Zhu, S., Li, W., Liu, J., Chen, C.H., Liao, Q., Xu, P., Xu, H., Xiao, T., Cao, Z., Peng, J., et al. (2016). Genome-scale deletion screening of human long non-coding RNAs using a paired-guide RNA CRISPR-Cas9 library. Nat Biotechnol *34*, 1279-1286. 10.1038/nbt.3715.
- 38. Chen, C., Yu, W., Tober, J., Gao, P., He, B., Lee, K., Trieu, T., Blobel, G.A., Speck, N.A., and Tan, K. (2019). Spatial Genome Re-organization between Fetal and Adult Hematopoietic Stem Cells. Cell Rep *29*, 4200-4211 e4207. 10.1016/j.celrep.2019.11.065.
- 39. Qi, Q., Cheng, L., Tang, X., He, Y., Li, Y., Yee, T., Shrestha, D., Feng, R., Xu, P., Zhou, X., et al. (2021). Dynamic CTCF binding directly mediates interactions among cis-regulatory elements essential for hematopoiesis. Blood *137*, 1327-1339. 10.1182/blood.2020005780.
- 40. Takayama, N., Murison, A., Takayanagi, S.I., Arlidge, C., Zhou, S., Garcia-Prat, L., Chan-Seng-Yue, M., Zandi, S., Gan, O.I., Boutzen, H., et al. (2021). The Transition from Quiescent to Activated States in Human Hematopoietic Stem Cells Is Governed by Dynamic 3D Genome Reorganization. Cell Stem Cell 28, 488-501 e410. 10.1016/j.stem.2020.11.001.
- 41. Hu, G., Cui, K., Fang, D., Hirose, S., Wang, X., Wangsa, D., Jin, W., Ried, T., Liu, P., Zhu, J., et al. (2018). Transformation of Accessible Chromatin and 3D Nucleome Underlies Lineage Commitment of Early T Cells. Immunity 48, 227-242 e228. 10.1016/j.immuni.2018.01.013.
- 42. Zhang, C., Xu, Z., Yang, S., Sun, G., Jia, L., Zheng, Z., Gu, Q., Tao, W., Cheng, T., Li, C., and Cheng, H. (2020). tagHi-C Reveals 3D Chromatin Architecture Dynamics during Mouse Hematopoiesis. Cell Rep 32, 108206. 10.1016/j.celrep.2020.108206.
- 43. Kloetgen, A., Thandapani, P., Ntziachristos, P., Ghebrechristos, Y., Nomikou, S., Lazaris, C., Chen, X., Hu, H., Bakogianni, S., Wang, J., et al. (2020). Three-dimensional chromatin landscapes in T cell acute lymphoblastic leukemia. Nat Genet *52*, 388-400. 10.1038/s41588-020-0602-9.
- 44. Luo, H., Wang, F., Zha, J., Li, H., Yan, B., Du, Q., Yang, F., Sobh, A., Vulpe, C., Drusbosky, L., et al. (2018). CTCF boundary remodels chromatin domain and drives aberrant HOX gene transcription in acute myeloid leukemia. Blood *132*, 837-848. 10.1182/blood-2017-11-814319.
- 45. Vilarrasa-Blasi, R., Soler-Vila, P., Verdaguer-Dot, N., Russinol, N., Di Stefano, M., Chapaprieta, V., Clot, G., Farabella, I., Cusco, P., Kulis, M., et al. (2021). Dynamics of genome architecture and chromatin function during human B cell differentiation and neoplastic transformation. Nat Commun *12*, 651. 10.1038/s41467-020-20849-y.
- 46. Xu, J., Song, F., Lyu, H., Kobayashi, M., Zhang, B., Zhao, Z., Hou, Y., Wang, X., Luan, Y., Jia, B., et al. (2022). Subtype-specific 3D genome alteration in acute myeloid leukaemia. Nature *611*, 387-398. 10.1038/s41586-022-05365-x.

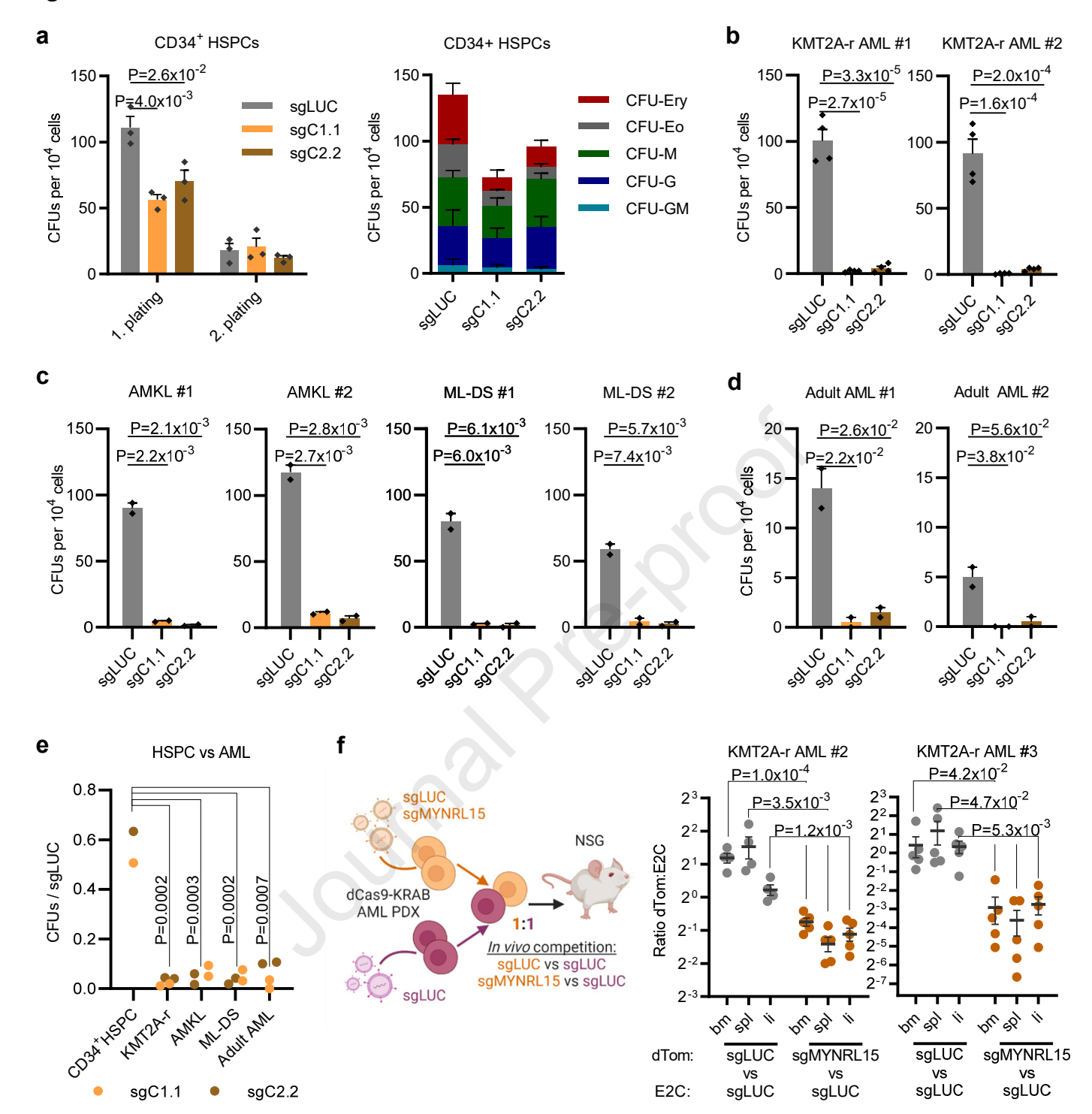
- 47. Hsieh, T.S., Fudenberg, G., Goloborodko, A., and Rando, O.J. (2016). Micro-C XL: assaying chromosome conformation from the nucleosome to the entire genome. Nat Methods *13*, 1009-1011. 10.1038/nmeth.4025.
- 48. Stemmer, M., Thumberger, T., Del Sol Keyer, M., Wittbrodt, J., and Mateo, J.L. (2015). CCTop: An Intuitive, Flexible and Reliable CRISPR/Cas9 Target Prediction Tool. PLoS One 10, e0124633. 10.1371/journal.pone.0124633.
- 49. Adams, F.F., Heckl, D., Hoffmann, T., Talbot, S.R., Kloos, A., Thol, F., Heuser, M., Zuber, J., Schambach, A., and Schwarzer, A. (2017). An optimized lentiviral vector system for conditional RNAi and efficient cloning of microRNA embedded short hairpin RNA libraries. Biomaterials *139*, 102-115. 10.1016/j.biomaterials.2017.05.032.
- 50. Al-Kershi, S., Bhayadia, R., Ng, M., Verboon, L., Emmrich, S., Gack, L., Schwarzer, A., Strowig, T., Heckl, D., and Klusmann, J.H. (2019). The stem cell-specific long noncoding RNA HOXA10-AS in the pathogenesis of KMT2A-rearranged leukemia. Blood Adv *3*, 4252-4263. 10.1182/bloodadvances.2019032029.
- 51. Emmrich, S., Rasche, M., Schoning, J., Reimer, C., Keihani, S., Maroz, A., Xie, Y., Li, Z., Schambach, A., Reinhardt, D., and Klusmann, J.H. (2014). miR-99a/100~125b tricistrons regulate hematopoietic stem and progenitor cell homeostasis by shifting the balance between TGFbeta and Wnt signaling. Genes Dev 28, 858-874. 10.1101/gad.233791.113.
- 52. Stein, C.A., Hansen, J.B., Lai, J., Wu, S., Voskresenskiy, A., Hog, A., Worm, J., Hedtjarn, M., Souleimanian, N., Miller, P., et al. (2010). Efficient gene silencing by delivery of locked nucleic acid antisense oligonucleotides, unassisted by transfection reagents. Nucleic Acids Res *38*, e3. 10.1093/nar/gkp841.
- 53. Harrow, J., Frankish, A., Gonzalez, J.M., Tapanari, E., Diekhans, M., Kokocinski, F., Aken, B.L., Barrell, D., Zadissa, A., Searle, S., et al. (2012). GENCODE: the reference human genome annotation for The ENCODE Project. Genome Res 22, 1760-1774. 10.1101/gr.135350.111.
- 54. Volders, P.J., Verheggen, K., Menschaert, G., Vandepoele, K., Martens, L., Vandesompele, J., and Mestdagh, P. (2015). An update on LNCipedia: a database for annotated human IncRNA sequences. Nucleic Acids Res *43*, 4363-4364. 10.1093/nar/gkv295.
- 55. Zhao, Y., Li, H., Fang, S., Kang, Y., Wu, W., Hao, Y., Li, Z., Bu, D., Sun, N., Zhang, M.Q., and Chen, R. (2016). NONCODE 2016: an informative and valuable data source of long noncoding RNAs. Nucleic Acids Res *44*, D203-208. 10.1093/nar/gkv1252.
- 56. Gilbert, L.A., Horlbeck, M.A., Adamson, B., Villalta, J.E., Chen, Y., Whitehead, E.H., Guimaraes, C., Panning, B., Ploegh, H.L., Bassik, M.C., et al. (2014). Genome-Scale CRISPR-Mediated Control of Gene Repression and Activation. Cell *159*, 647-661. 10.1016/j.cell.2014.09.029.
- 57. Concordet, J.P., and Haeussler, M. (2018). CRISPOR: intuitive guide selection for CRISPR/Cas9 genome editing experiments and screens. Nucleic Acids Res *46*, W242-W245. 10.1093/nar/gky354.
- 58. Labuhn, M., Adams, F.F., Ng, M., Knoess, S., Schambach, A., Charpentier, E.M., Schwarzer, A., Mateo, J.L., Klusmann, J.H., and Heckl, D. (2018). Refined sgRNA efficacy prediction improves large- and small-scale CRISPR-Cas9 applications. Nucleic Acids Res *46*, 1375-1385. 10.1093/nar/gkx1268.
- Love, M.I., Huber, W., and Anders, S. (2014). Moderated estimation of fold change and dispersion for RNA-seq data with DESeq2. Genome Biol 15, 550. 10.1186/s13059-014-0550-8
- 60. Bhayadia, R., Krowiorz, K., Haetscher, N., Jammal, R., Emmrich, S., Obulkasim, A., Fiedler, J., Schwarzer, A., Rouhi, A., Heuser, M., et al. (2018). Endogenous Tumor Suppressor microRNA-193b: Therapeutic and Prognostic Value in Acute Myeloid Leukemia. J Clin Oncol 36, 1007-1016. 10.1200/JCO.2017.75.2204.
- 61. Kim, D., Paggi, J.M., Park, C., Bennett, C., and Salzberg, S.L. (2019). Graph-based genome alignment and genotyping with HISAT2 and HISAT-genotype. Nat Biotechnol *37*, 907-915. 10.1038/s41587-019-0201-4.

- 62. Liao, Y., Smyth, G.K., and Shi, W. (2014). featureCounts: an efficient general purpose program for assigning sequence reads to genomic features. Bioinformatics *30*, 923-930. 10.1093/bioinformatics/btt656.
- 63. Subramanian, A., Tamayo, P., Mootha, V.K., Mukherjee, S., Ebert, B.L., Gillette, M.A., Paulovich, A., Pomeroy, S.L., Golub, T.R., Lander, E.S., and Mesirov, J.P. (2005). Gene set enrichment analysis: a knowledge-based approach for interpreting genome-wide expression profiles. Proc Natl Acad Sci U S A *102*, 15545-15550. 10.1073/pnas.0506580102.
- 64. Huang da, W., Sherman, B.T., and Lempicki, R.A. (2009). Systematic and integrative analysis of large gene lists using DAVID bioinformatics resources. Nat Protoc *4*, 44-57. 10.1038/nprot.2008.211.
- 65. Hughes, J.R., Roberts, N., McGowan, S., Hay, D., Giannoulatou, E., Lynch, M., De Gobbi, M., Taylor, S., Gibbons, R., and Higgs, D.R. (2014). Analysis of hundreds of cis-regulatory landscapes at high resolution in a single, high-throughput experiment. Nat Genet *46*, 205-212. 10.1038/ng.2871.
- 66. Buckle, A., Gilbert, N., Marenduzzo, D., and Brackley, C.A. (2019). capC-MAP: software for analysis of Capture-C data. Bioinformatics *35*, 4773-4775. 10.1093/bioinformatics/btz480.
- 67. Kent, W.J., Sugnet, C.W., Furey, T.S., Roskin, K.M., Pringle, T.H., Zahler, A.M., and Haussler, D. (2002). The human genome browser at UCSC. Genome Res *12*, 996-1006. 10.1101/gr.229102.
- 68. Knight, P.A., and Ruiz, D. (2012). A fast algorithm for matrix balancing. IMA Journal of Numerical Analysis 33, 1029-1047. 10.1093/imanum/drs019.
- 69. Krietenstein, N., Abraham, S., Venev, S.V., Abdennur, N., Gibcus, J., Hsieh, T.S., Parsi, K.M., Yang, L., Maehr, R., Mirny, L.A., et al. (2020). Ultrastructural Details of Mammalian Chromosome Architecture. Mol Cell *78*, 554-565 e557. 10.1016/j.molcel.2020.03.003.
- 70. Rao, S.S., Huntley, M.H., Durand, N.C., Stamenova, E.K., Bochkov, I.D., Robinson, J.T., Sanborn, A.L., Machol, I., Omer, A.D., Lander, E.S., and Aiden, E.L. (2014). A 3D map of the human genome at kilobase resolution reveals principles of chromatin looping. Cell *159*, 1665-1680. 10.1016/j.cell.2014.11.021.
- 71. Cabianca, D.S., Casa, V., Bodega, B., Xynos, A., Ginelli, E., Tanaka, Y., and Gabellini, D. (2012). A long ncRNA links copy number variation to a polycomb/trithorax epigenetic switch in FSHD muscular dystrophy. Cell *149*, 819-831. 10.1016/j.cell.2012.03.035.
- 72. Brinkman, E.K., Chen, T., Amendola, M., and van Steensel, B. (2014). Easy quantitative assessment of genome editing by sequence trace decomposition. Nucleic Acids Res *42*, e168. 10.1093/nar/gku936.
- 73. The Cancer Genome Atlas Research Network, Ley, T.J., Miller, C., Ding, L., Raphael, B.J., Mungall, A.J., Robertson, A., Hoadley, K., Triche, T.J., Jr., Laird, P.W., et al. (2013). Genomic and epigenomic landscapes of adult de novo acute myeloid leukemia. N Engl J Med *368*, 2059-2074. 10.1056/NEJMoa1301689.
- 74. Bolouri, H., Farrar, J.E., Triche, T., Jr., Ries, R.E., Lim, E.L., Alonzo, T.A., Ma, Y., Moore, R., Mungall, A.J., Marra, M.A., et al. (2018). The molecular landscape of pediatric acute myeloid leukemia reveals recurrent structural alterations and age-specific mutational interactions. Nat Med *24*, 103-112. 10.1038/nm.4439.
- 75. Leek, J.T., Johnson, W.E., Parker, H.S., Jaffe, A.E., and Storey, J.D. (2012). The sva package for removing batch effects and other unwanted variation in high-throughput experiments. Bioinformatics *28*, 882-883. 10.1093/bioinformatics/bts034.
- 76. van der Maaten, L.J.P.H., G. E. (2008). Visualizing high-dimensional data using t-SNE. J Mach Learn Res *9*, 2579-2605.









Highlights

- Long noncoding RNA locus MYNRL15 identified as a myeloid leukemia dependency
- MYNRL15 function is RNA-independent, mediated by two regulatory elements in locus
- Perturbation causes long-range looping, downregulation of cancer dependency genes
- Perturbation is anti-leukemic in primary AML cells from different genetic backgrounds



KEY RESOURCES TABLE

The table highlights the reagents, genetically modified organisms and strains, cell lines, software, instrumentation, and source data **essential** to reproduce results presented in the manuscript. Depending on the nature of the study, this may include standard laboratory materials (i.e., food chow for metabolism studies, support material for catalysis studies), but the table is **not** meant to be a comprehensive list of all materials and resources used (e.g., essential chemicals such as standard solvents, SDS, sucrose, or standard culture media do not need to be listed in the table). **Items in the table must also be reported in the method details section within the context of their use.** To maximize readability, the number of **oligonucleotides and RNA sequences** that may be listed in the table is restricted to no more than 10 each. If there are more than 10 oligonucleotides or RNA sequences to report, please provide this information as a supplementary document and reference the file (e.g., See Table S1 for XX) in the key resources table.

Please note that ALL references cited in the key resources table must be included in the main references list. Please report the information as follows:

- **REAGENT or RESOURCE:** Provide the full descriptive name of the item so that it can be identified and linked with its description in the manuscript (e.g., provide version number for software, host source for antibody, strain name). In the experimental models section (applicable only to experimental life science studies), please include all models used in the paper and describe each line/strain as: model organism: name used for strain/line in paper: genotype. (i.e., Mouse: OXTR^{fl/fl}: B6.129(SJL)-Oxtr^{tm1.1Wsy/J}). In the biological samples section (applicable only to experimental life science studies), please list all samples obtained from commercial sources or biological repositories. Please note that software mentioned in the methods details or data and code availability section needs to also be included in the table. See the sample tables at the end of this document for examples of how to report reagents.
- **SOURCE:** Report the company, manufacturer, or individual that provided the item or where the item can be obtained (e.g., stock center or repository). For materials distributed by Addgene, please cite the article describing the plasmid and include "Addgene" as part of the identifier. If an item is from another lab, please include the name of the principal investigator and a citation if it has been previously published. If the material is being reported for the first time in the current paper, please indicate as "this paper." For software, please provide the company name if it is commercially available or cite the paper in which it has been initially described.
- IDENTIFIER: Include catalog numbers (entered in the column as "Cat#" followed by the number, e.g., Cat#3879S). Where available, please include unique entities such as RRIDs, Model Organism Database numbers, accession numbers, and PDB, CAS, or CCDC IDs. For antibodies, if applicable and available, please also include the lot number or clone identity. For software or data resources, please include the URL where the resource can be downloaded. Please ensure accuracy of the identifiers, as they are essential for generation of hyperlinks to external sources when available. Please see the Elsevier Ist of data repositories with automated bidirectional linking for details. When listing more than one identifier for the same item, use semicolons to separate them (e.g., Cat#3879S; RRID: AB 2255011). If an identifier is not available, please enter "N/A" in the column.
 - A NOTE ABOUT RRIDs: We highly recommend using RRIDs as the identifier (in particular for antibodies and organisms but also for software tools and databases). For more details on how to obtain or generate an RRID for existing or newly generated resources, please <u>visit the RII</u> or <u>search for RRIDs</u>.

Please use the empty table that follows to organize the information in the sections defined by the subheading, skipping sections not relevant to your study. Please do not add subheadings. To add a row, place the cursor at the end of the row above where you would like to add the row, just outside the right border of the table. Then press the ENTER key to add the row. Please delete empty rows. Each entry must be on a separate row; do not list multiple items in a single table cell. Please see the sample tables at the end of this document for relevant examples in the life and physical sciences of how reagents and instrumentation should be cited.



TABLE FOR AUTHOR TO COMPLETE

Please upload the completed table as a separate document. <u>Please do not add subheadings to the key resources table.</u> If you wish to make an entry that does not fall into one of the subheadings below, please contact your handling editor. <u>Any subheadings not relevant to your study can be skipped.</u> (NOTE: References within the KRT should be in numbered style rather than Harvard.)

Key resources table

REAGENT or RESOURCE	SOURCE	IDENTIFIER
Antibodies		
Anti-human CD45-FITC (clone J33)	Beckman Coulter	Cat# A07782; RRID:AB_10645157
Bacterial and virus strains	(.	
XL1-Blue supercompetent cells	Agilent	Cat# 200236
Subcloning efficiency DH5a competent cells	Invitrogen	Cat# 18265017
Biological samples		
Healthy CD34 ⁺ HSPCs	This paper	N/A
Patient derived xenografts (Table S5)	This paper	N/A
Chemicals, peptides, and recombinant proteins		
Recombinant human SCF	Peprotech	Cat# 300-07
Recombinant human FLT3L	Peprotech	Cat# 300-19
Recombinant human IL-3	Peprotech	Cat# 200-03
Recombinant human IL-6	Peprotech	Cat# 200-06
Recombinant human TPO	Peprotech	Cat# 300-18
Recombinant human GM-CSF	Peprotech	Cat# 300-03
StemRegenin 1	STEMCELL	Cat# 72344
UM171	STEMCELL	Cat# 72914
RetroNectin® recombinant human fibronectin fragment	TaKaRa Bio	Cat# T100B
Lenti-X [™] concentrator	TaKaRa Bio	Cat# 631231
Polybrene	Sigma Aldrich	Cat# TR-1003-G
Critical commercial assays		
Plasmid maxi kit	Qiagen	Cat# 12163
QIAamp DNA blood mini kit	Qiagen	Cat# 51104
NEBNext® high-fidelity PCR master mix	New England Biolabs	Cat# M0541L
Human methylcellulose complete media	R&D Systems	Cat# HSC003
Dual-luciferase® reporter assay system	Promega	Cat# E1910
High-capacity cDNA reverse transcription kit	Applied Biosystems	Cat# 4368814
SYBR [™] select master mix	Applied Biosystems	Cat# 4472908
Deposited data		
Raw and processed RNA-seq, Capture-C data	This paper	GEO: GSE172240
Raw amplicon sequence data from CRISPR screens	This paper	ENA: PRJEB44308, PRJEB44320
Experimental models: Cell lines		
HEK293T	DSMZ	DSMZ# ACC 635; RRID:CVCL_0063
K562	DSMZ	DSMZ# ACC 10; RRID:CVCL_0004



ML-2	DSMZ	DSMZ# ACC 15;
IVIL-Z	DOIVIZ	RRID:CVCL_1418
M-07E	DSMZ	DSMZ# ACC 104;
		RRID:CVCL_2106
KASUMI-1	DSMZ	DSMZ# ACC 220;
		RRID:CVCL_0589
NOMO-1	DSMZ	DSMZ# ACC 542;
0/0/0 4	DOMZ	RRID:CVCL_1609
SKNO-1	DSMZ	DSMZ# ACC 690; RRID:CVCL 2196
OCI-AML3	DSMZ	DSMZ# ACC 582;
OCI-AIVILO	DOIVIZ	RRID:CVCL_1844
TF-1	DSMZ	DSMZ# ACC 334;
		RRID:CVCL_0559
NB-4	DSMZ	DSMZ# ACC 207;
		RRID:CVCL_0005
Experimental models: Organisms/strains		
Mus musculus: NOD.Cg-Prkdcscid II2rgtm1Wjl/SzJ	Charles River	RRID:IMSR_JAX:00
	Laboratories	5557
Oligonucleotides		
sgRNA library sequences (Tables S1-S3)	This paper	N/A
sgRNA, shRNA, LNA-gapmeR sequences (Table S6)	This paper	N/A
PCR and qPCR primers (Table S6)	This paper	N/A
Capture-C probes (Table S6)	This paper	N/A
Negative control B LNA-gapmeR	Qiagen	Cat# 339515
QuantiTect® primer assay for IMP3	Qiagen	Cat# QT00232330
QuantiTect® primer assay for WDR61	Qiagen	Cat# QT00083776
Recombinant DNA	J	
psPAX2	N/A	Addgene# 12260
pMD2.G	N/A	Addgene# 12259
SGL40C.EFS.dTomato	Reimer et al. 2017	Addgene# 89395
SGL40C.EFS.E2Crimson	Labuhn et al. 2018	Addgene# 100894
SGL40C.mU6.EFS.RFP657	This paper	Addgene# 207866
SIN40C.SFFV.eGFP.miR30n	Alejo-Valle et al. 2022	Addgene# 169278
LBid.Inc.GFP	Al-Kershi et al. 2019	N/A
L40C-CRISPR.EFS.mNeon	Reimer et al. 2017	Addgene# 69146
pLKO5d.SFFV.dCas9-KRAB.P2A.BSD	Schwarzer et al. 2017	Addgene# 90332
pLKO5d.EFS.SpCas9.P2A.BSD	Heckl et al. 2014	Addgene# 57821
SIN40C.SFFV.dCas9-KRAB.P2A.mNeon	This paper	Addgene# 170482
SGL.EFS.tBFP	This paper	Addgene# 173915
pAG/MNase	Meers <i>et al.</i> , 2019	Addgene# 123461
pGL4.23	Promega	Cat# E8411
·	1 Tomoga	Julii EUTTI
Software and algorithms	CranhDad	https://www.anaalaaa
GraphPad Prism	GraphPad	https://www.graphpa d.com/scientific-
		software/prism/;
		RRID:SCR_002798
FlowJo	BD Biosciences	https://www.flowjo.co
		m/solutions/flowjo;
		RRID:SCR_008520



Kaluza	Beckman Coulter	https://www.beckma
		n.com/flow-
		cytometry/software/k
		aluza;
0.07	0:	RRID:SCR_016182
ССТор	Stemmer et al. 2015	https://cctop.cos.uni-
		heidelberg.de/; RRID:SCR_016890
CRISPOR	Concordet and	http://crispor.tefor.ne
ORIGI OR	Haeussler, 2018	t/;
		RRID:SCR_015935
MAGeCK	Li et al. 2014	https://sourceforge.n
		et/p/mageck/wiki/
TIDE	Brinkman et al. 2014	http://shinyapps.data
'D.M	A 1	curators.nl/tide/
miR-N	Adams et al. 2017	http://shinyapps.data curators.nl/tide/
R	R project	https://www.r-
TX .	it project	project.org/about.ht
		ml;
		RRID:SCR_001905
R: DESeq2	Love et al. 2014	https://bioconductor.
. (org/packages/releas
		e/bioc/html/DESeq2.
		html;
R: sva	Leek et al., 2012	RRID:SCR_015687 https://bioconductor.
N. SVa	Leek et al., 2012	org/packages/releas
		e/bioc/html/sva.html;
		RRID:SCR_012836
R: Rtsne	van der Maaten and	https://cran.r-
	Hinton, 2008	project.org/web/pack
		ages/Rtsne/index.ht
		ml; RRID:SCR_016342
GSEA	Subramanian et al.,	https://www.gsea-
COLA	2005	msigdb.org/gsea/ind
		ex.jsp;
		RRID:SCR_003199
MSigDB	Liberzon et al. 2015	https://www.gsea-
		msigdb.org/gsea/msi
		gdb/index.jsp;
DAVID	Sherman et al. 2022	RRID:SCR_016863 https://david.ncifcrf.g
	Oneman & al. 2022	ov/home.jsp
CapSequm2	Hughes et al., 2014	https://capsequm.mo
	3, .	lbiol.ox.ac.uk/cgi-
		bin/CapSequm.cgi
capC-MAP	Buckle et al., 2019	https://capc-
		map.readthedocs.io/
101/	Debineen of al 2014	en/latest/
IGV	Robinson et al. 2011	https://software.broa dinstitute.org/softwar
		e/igv/;
		RRID:SCR_011793
	L	



UCSC genome browser	Kent et al. 2002	https://genome.ucsc.
Cooc genome browser	Nent et al. 2002	edu/;
		RRID:SCR_005780
Other		
Ensembl gene, transcript, CDS annotations	Ensembl	http://www.ensembl.
		org/index.html;
		RRID:SCR_002344
K562 ChIP-seq data: H3K4Me3, H3K4Me1, H3K27Ac,	ENCODE	https://www.encodep
CTCF, SMC3, AGO1, BHLHE40, E2F6, EGR1, ESRRA, GABPB1, GMEB1, HNRNPLL, IRF1, L3MBTL2, MAX,		roject.org/; RRID:SCR_015482;
MNT, NRF1, PHF20, PHF8, PML, PRDM10, RBFOX2,		ENCFF767UON,
RLF, RNF2, SAP30, TBP, THRA, ZBTB7A, ZNF639		ENCFF759NWD,
		ENCFF038DDS,
		ENCFF519CXF,
	X	ENCFF175UEE,
		ENCFF100VYA,
		ENCFF477JTV, ENCFF533GSH,
		ENCFF335G5H, ENCFF375RDB,
		ENCFF592GWM,
		ENCFF700DXR,
		ENCFF678VPQ,
. (ENCFF662WPN,
		ENCFF978BBL,
		ENCFF423LPW, ENCFF618VMC,
		ENCFF926CRV,
		ENCFF543STN,
		ENCFF259HUS,
		ENCFF952YDR,
		ENCFF800QDU,
		ENCFF600HPZ,
		ENCFF232ASB, ENCFF599CBB,
		ENCFF349MSP,
		ENCFF103RHL,
		ENCFF370YGS,
		ENCFF309DMZ,
		ENCFF245LRG,
H4 hECC Micro C and VECC VDM7, CM40070, NULTIV	4DN	ENCFF404EVY
H1-hESC Micro-C and K562, KBM7, GM12878, NHEK, HUVEC, HMEC, IMR90 Hi-C data	4DN	https://data.4dnucleome.org/;
Tioves, Finites, Invites in Studies		RRID:SCR 016925;
		4DNFI2TK7L2F,
		4DNESI7DEJTM,
		4DNESDEK4IH8,
		4DNES3JX38V5,
		4DNESECNR4O8,
		4DNESHFBC56P,
		4DNESIE5R9HS, 4DNES1ZEJNRU
Genome-wide CRISPR screening data	DepMap	https://depmap.org/p
, and the second		ortal/download
TCGA AML RNA-seq data	TCGA	https://gdc.cancer.go
		v/access-data



TARGET AML RNA-seq data	TARGET	https://ocg.cancer.go v/programs/target/da ta-matrix
LncScape expression data	Schwarzer et al. 2017	https://ag- klusmann.shinyapps. io/lncScape/